Observations of Atmospheric Methane and Carbon Dioxide Mixing Ratios: Tall-Tower or Mountain-Top Stations?

Journal Article

Author(s):
Bamberger, Ines; Oney, Brian; Brunner, Dominik; Henne, Stephan; Leuenberger, Markus; Buchmann, Nina; Eugster, Werner

Publication date:
2017-07

Permanent link:
https://doi.org/10.3929/ethz-b-000218213

Originally published in:
Boundary-Layer Meteorology 164(1), https://doi.org/10.1007/s10546-017-0236-3

Funding acknowledgement:
136273 - CarboCount CH: Quantifying greenhouse gas fluxes and their sensitivity to climate variations: A case study in Central Europe and Switzerland (SNF)

Observations of Atmospheric Methane and Carbon Dioxide Mixing Ratios: Tall-tower or Mountain-top Stations?

Ines Bamberger • Brian Oney • Dominik Brunner • Stephan Henne • Markus Leuenberger • Nina Buchmann • Werner Eugster

Received: DD Month 2015/ Accepted: DD Month YEAR

Abstract Mountain-top observations of greenhouse gas mixing ratios may be an alternative to tall-tower measurements for regional scale source and sink estimation. To investigate the equivalence or limitations of a mountain-top site as compared to a tall tower site, we used the unique opportunity of comparing in situ measurements of methane (CH_4) and carbon dioxide (CO_2) mixing ratios at a mountain top (986 m above sea level, a.s.l.) with measurements from a nearby (distance 28.4 km) tall tower, sampled at almost the same elevation (1009 m a.s.l.). Special attention was given to (i) how local wind statistics and greenhouse gas sources and sinks at the mountain top influence the observations, and (ii) whether mountain-top observations can be used as for those from a tall tower for constraining regional greenhouse gas emissions. Wind statistics at the mountain-top site are clearly more influenced by local flow systems than those at the tall-tower site. Differences in temporal patterns of the greenhouse gas mixing ratios observed at the two sites are mostly related to the influence of local sources and sinks at the

Ines Bamberger • Nina Buchmann • Werner Eugster
Department of Environmental Systems Science, Institute of Agricultural Sciences, ETH Zurich, Switzerland.
e-mail: {ines.bamberger@kit.edu}, {eugsterw@ethz.ch}

Present Address
Ines Bamberger
Institute of Meteorology and Climate Research Atmospheric Environmental Research (IMK-IFU), Karlsruhe Institute of Technology (KIT), Campus Alpin, Garmisch-Partenkirchen, Germany

Brian Oney • Dominik Brunner • Stephan Henne
Empa, Swiss Federal Laboratories for Materials Science and Technology, Duebendorf, Switzerland.

Markus Leuenberger
Physics Institute, Climate and Environmental Physics, University of Bern, Switzerland

mountain top site. Major influences of local sources can be removed by applying a statistical filter (5th percentile) or a filter that removes periods with unfavourable flow conditions. In the best case, the bias in mixing ratios between the mountain-top and the tall-tower sites after the application of the wind filter was –0.0005 ± 0.0010 ppm for methane (September, 0000–0400 UTC) and 0.11 ± 0.18 ppm for CO_2 (February, 1200–1600 UTC). Temporal fluctuations of atmospheric CH_4 and CO_2 mixing ratios at both stations also showed good agreement (apart from CO_2 during summertime) as determined by moving bi-weekly Pearson correlation coefficients (up to 0.96 for CO_2 and 0.97 for CH_4). When only comparing mixing ratios minimally influenced by local sources (low bias and high correlation coefficients), our measurements indicate that mountain-top observations are comparable to tall-tower observations.

Keywords Atmospheric observations · Greenhouse gases · Local greenhouse gas sources · Mountain meteorology · Mountain top · Tall tower

1 Introduction

Tall-tower measurements of atmospheric greenhouse gases contain information from larger spatial scales than measurements close to the ground (Marquis and Tans 2008) and thus provide valuable information for resolving regional transport and the distribution of greenhouse gases (Gloor et al., 2001). In contrast, greenhouse gas mixing ratios measured at mountain-top stations are often more influenced by boundary-layer processes and by local sources and sinks than are tall-tower measurements. This is mainly due to the complex topography around mountain sites and the low sampling height above the ground, allowing local fluxes to considerably influence the local concentration field. To address the question: how similar, or how different, are mountain-top and tall-tower measurements at the same elevation above sea level, we compared carbon dioxide (CO_2) and methane (CH_4) mixing ratio measurements at a mountain-top and a tall-tower site that are only separated by 28.4 km, which allows for a unique and direct comparison. It is not expected that short-term variations at two sites separated by such a distance are synchronous, but it can be expected that, with adequate statistical aggregation,

measurements made at both sites should provide similar regional information in the CO_2 and CH_4 time series.

While the global budgets of carbon dioxide and methane are relatively well known, their sources and sinks are poorly constrained based on current regional scale observational networks, where "regional" used herein refers to an area > 10^4 km^2 (Cleugh et al. 2004). With a joint contribution of 81 % to the positive anthropogenic radiative forcing, CO_2 and CH_4 are the two most important anthropogenic greenhouse gases (Myhre et al. 2013). Even though tall-tower networks in both Europe and North America provide observations of net changes in CO_2 and CH_4 mixing ratios at large spatial scales, the network density is insufficient to resolve atmospheric and surface flux patterns at the smaller regional (sub-national) scale (Marquis and Tans 2008, Villani et al. 2010, Dlugokencky et al. 2011). An increased number of tall-tower stations would be beneficial for resolving the regional distribution of greenhouse gas mixing ratios (Lauvaux et al. 2012). A concentrated effort towards a dense regional network of tall towers was initiated by the NOAA Earth System Research Laboratory that resulted in a network of seven towers (Andrews et al. 2014). Similarly in Europe, a tall tower network exists with seven towers (e.g., Vermeulen et al. 2011, Thompson et al. 2009), and in order to expand existing and create new networks, TV and radio broadcasting towers could be equipped with relevant instrumentation (Marquis and Tans 2008, Andrews et al. 2014). Such towers and additional sites are currently being integrated into the European Integrated Carbon Observation System (ICOS, www.icos-ri.eu). However, access to existing telecommunication towers may not always be possible, and the installation and maintenance of measurement instrumentation is often prohibitive and time intensive.

Other approaches such as aircraft measurements (e.g., Beck et al. 2012, Schuck et al. 2012, Xiong et al. 2010) yield useful snapshots of the atmospheric composition and add supplementary information on vertical and horizontal profiles (Crevoisier et al. 2006, Zhang et al. 2014). Long-term aircraft measurements of greenhouse gases within the NOAA atmospheric monitoring network have been carried out by Karion et al. (2013) twice a week over selected areas, but such airborne measurements cannot provide continuous, long-term observations, and may miss essential parts of the atmospheric variability, especially on the regional scale. Remote sensing products such as satellite

retrievals of global atmospheric greenhouse gas total column mixing ratios have recently become available (Frankenberg et al. 2005, 2008, 2015, Kuze et al. 2009, Buchwitz et al. 2013). These measurements are complementary in their ability to provide spatial information on atmospheric greenhouse gases. However, they are still limited in their temporal and spatial resolutions, are affected by cloud cover, and are less accurate and less sensitive to surface fluxes than in situ measurements (Marquis and Tans 2008). Alternatively, continuous measurements of CO_2 and CH_4 mixing ratios close to the ground but at elevated locations such as mountain tops might provide a footprint of similar size as that of a tall-tower station. Consequently, the use of such measurement stations could complement the number of sites used to measure greenhouse gas mixing ratios, especially in mountainous regions where tower facilities are rare (Andrews et al. 2014, Lee et al. 2015). However, to the best of our knowledge, the comparability of mountain-top data to tall-tower data in a direct comparison, as we present here, has not yet been investigated. Greenhouse gas mixing ratios at mountain tops might be influenced by local flows and nearby greenhouse gas sources and sinks. All these influences may negatively affect the regional representativeness of mountain top measurements (Brooks et al. 2012). Before being used in atmospheric inversions, mountain-top measurements may need to be screened using meteorological or statistical filters in order to remove local influences (Brooks et al. 2012, Lee et al. 2015).

Highly accurate atmospheric mixing ratio measurements in combination with an inverse transport model are required to produce quantitative information on greenhouse gas sources and sinks (Nisbet and Weiss 2010). Thus, apart from network density and accuracy of measurements, the top-down approach to determining regional and global greenhouse gas fluxes is dependent on the reliability of transport models to allocate regional sources and sinks (Lin and Gerbig 2005, Gerbig et al. 2008, Tolk et al. 2008, Kretschmer et al. 2014). Even if measurements are taken at considerable altitudes above ground, the exact representation of the transport of greenhouse gases may be a major source of uncertainty in these top-down approaches (e.g., McKain et al. 2012, Smallman et al. 2014). Especially due to the development of small-scale local circulations, such as thermally induced slope-wind systems (Whiteman 2000) and their insufficient representation in relatively coarse-resolution atmospheric transport models, the

greenhouse gas mixing ratios above complex terrain (e.g. mountain tops) are difficult to predict using such models. Subgrid-scale transport processes due to complex topography are currently not, or only very crudely, represented in global and regional-scale transport models (van der Molen and Dolman 2007, Tolk et al. 2008) that are used for estimating greenhouse gas fluxes at continental to global scales. Recently it has been argued that the use of such coarse transport models results in an underestimation of net CO_2 exchange (Rotach et al. 2013), which is critical since at least 50 % of the land surface can be classified as complex terrain (Rotach et al. 2007, 2013). Thus, in combination with measurements in complex terrain (e.g. at mountain tops), high-resolution transport models are required to capture micro scale to meso scale (2 to 20 km) wind circulations and their effect on greenhouse gas mixing ratios (Pillai et al. 2011). Another drawback of mountain-top measurements may be that they are affected by microscale greenhouse gas sources or sinks, close to the measurement inlet that cannot readily be represented in a transport model. Thus, it is unclear how local sources and local flows will influence greenhouse gas mixing ratios observed at a mountain-top station as compared to a tall-tower station.

The aim of this study is to determine whether a mountain-top station can provide data of similar quality as those at a tall-tower station. For this purpose, we compared CO_2 and CH_4 mixing ratio measurements at sub-daily to seasonal time scales from a tall-tower and a mountain-top station in Switzerland, located at a similar elevation (above sea level) and with a relatively short horizontal distance from each other (28.4 km). The two sites are part of a greenhouse gas observation network in Switzerland that has recently been established in the framework of the CarboCount CH project (www.carbocount.ch, Oney et al. 2015).

We pose the following questions: (1) How different are flows at the mountain-top compared to the tall-tower stations? (2) How important is the potential contamination of the mountain-top measurements by local greenhouse gas sources and sinks if an inlet close to the ground is used? (3) Is it possible to identify optimum atmospheric conditions for which mountain-top observations are comparable to those from a tall tower, given that other environmental factors are similar (i.e. climate, distance to pollution from urban centres)?

2 Materials and Methods

2.1 Field Sites

Measurements of greenhouse gases and meteorological variables were made at two of the four sites of the CarboCount CH observation network in Switzerland, which has been established to investigate greenhouse gas sources and sinks through an integrated approach using both observations and atmospheric transport models (Oney et al. 2015). The two sites are located within 28.4 km of each other close to the southern edge of the Swiss Plateau, the relatively flat, most densely populated and agriculturally used area in Switzerland, located between the Alps and the Jura mountains. A cross-sectional profile of the topography between both stations and photographs of the corresponding sites are shown in Fig. 1. The proximity of both sites guaranteed comparable weather conditions as well as a similar distance to major greenhouse gas sources and sinks.

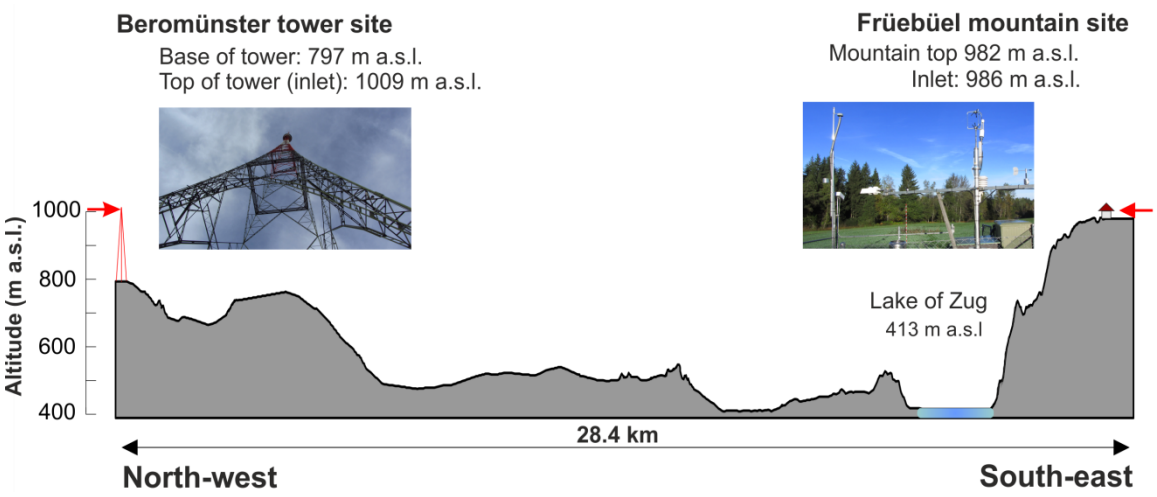

Fig. 1 Topographical transect between the tall-tower site Beromünster (left) and the mountain-top site Früebüel (right). Red arrows indicate the inlet heights at both sites. Note the vertical amplification of the scale.

2.1.1 Früebüel Mountain-top Station

Measurements at Früebüel – a Swiss FluxNet site (www.swissfluxnet.ch) – were taken on top of the Zugerberg mountain ridge, located at an elevation of 982 m above sea level

(a.s.l.) in the pre-alpine foothills of Switzerland (47°06′57.0″ N, 8°32′16.0″ E). The site is located on a relatively flat highland, extending about 2 km in the east–west and 5 km in the north–south directions, and is thus not a classical mountain-top site because it has no pronounced peak. Average daytime convective boundary-layer heights above the Swiss Plateau usually exceed 500 m above the ground during the warm season (March to September, Collaud Coen et al. 2014). With an elevation of 1000 m (≈ 500 m above the Swiss Plateau) we therefore assume that Früebüel mostly lies within the convective boundary layer.

The Zugerberg mountain ridge is a sparsely populated agricultural area, with prevailing land-cover types managed grasslands and forests. The towns of Zug (at ≈ 10 km distance) and Lucerne (≈ 20 km) are the nearest larger towns and are situated approximately 450 m below the measurement station's elevation.

The air inlet for the greenhouse gas mixing ratio measurements was installed 4 m above a moderately intensively managed grassland (Zeeman et al. 2010, Imer et al. 2013), with meteorological measurements (wind speed, air temperature) taken approximately 3 m away from the air inlet at 2-m height. In 2013, the average air temperature was 7.1 °C, ranging from –14.5 °C to 34.8 °C (range of 2-h averages).

Farmsteads and barns of the ETH (*Eidgenössische Technische Hochschule*) research station Früebüel are located approximately 300 m to the south-west of the atmospheric measurement tower. In 2013, the farmstead accommodated between 96 (June) and 50 (December) head of cattle, and from October till mid-November an additional 15 sheep. From mid-July to mid-September all cattle were relocated to remote alpine pastures off site. Otherwise, there were no other farmsteads or other anthropogenic sources in close vicinity to the site. The three grassland parcels directly adjacent to the station were managed differently; while the ungrazed meadow next to the measurement station was cut three times and fertilized twice a year, the two grazed parcels were only fertilized once and cut once or twice a year (Table S1 in Supplementary Material).

2.1.2 Beromünster Tall-Tower Station

The Beromünster tall-tower station is located approximately 30 km to the west of Früebüel, atop a gentle hill (797 m a.s.l., 47°11′22.4″N, 8°10′31.5″E) close to Lake Sempach, Switzerland. The area surrounding the tall-tower station is predominantly used for agriculture. The two larger towns closest to the tall tower are Lucerne (≈ 20 km) and Zug (≈ 30 km). The tall tower is the taller of two former national radio broadcast towers and is protected as a national monument, and is no longer used for telecommunication. Although greenhouse gas and meteorological measurements were made at five different heights, we have only used measurements from the top of the tower at an elevation of 1009 m a.s.l. (212 m above ground level), similar to the elevation of measurements at Früebüel. Air temperatures recorded at this elevation ranged from –9.9 °C to 29.1 °C in the year 2013, resulting in an annual average of 7.3 °C.

2.2 Instrumentation

Mixing ratios of CO_2 and CH_4 at the mountain-top station (Früebüel) were measured with a cavity ring-down spectrometer (Picarro G2301, Picarro Inc., Santa Clara, California, USA), while the tall-tower station (Beromünster) was equipped with a Picarro G2401 analyzer that also measured CO mixing ratios. Both instruments were operated at a standard cavity pressure of 186.7 hPa and a cavity temperature of 45 °C. All times reported here are given in UTC, which differs by one hour from local time (CET–1 h).

Früebüel: The air inlet was covered by an inlet filter (F-15-050, Solberg International, Ltd., Itasca, IL, USA). Ambient air was drawn through an insulated and heated Synflex 1300 hose to the analyzer, which was placed within an air-conditioned (20–28 °C) container. Automatic recalibration of the system was performed daily using three reference gases (high: CO_2/CH_4 mixing ratios 475.3/2.398 ppm; low: 383.5/1.895 ppm; working: 405.2/2.056 ppm). Calibration gases were traced to the WMO primary standards WMO-X2007 for CO_2 and WMO-X2004 for CH_4. The accuracy of the greenhouse gas measurements was estimated at ≤ 0.07 ppm and ≤ 0.0005 ppm for CO_2 and CH_4, respectively (Oney et al. 2015). Details about the meteorological sensors are given by Zeeman et al. (2010).

Beromünster: At the Beromünster tall tower, air was drawn at a flow rate of 14 L min^{-1} from the highest level (212 m) to the analyzer through a 220 m long inlet tube. The analyzer was placed within the old radio transmitter building at the base of the tower, and automatic calibration was done once a week (high: 472.66/2.4247 ppm; low: 382.11/1.9089 ppm) similarly to Früebüel. In addition, every 6 h measurements were compared with a working gas standard (392.24/2.1312 ppm), see Berhanu et al. (2016).

Meteorological measurements at the highest level of the tall tower were provided by an integrated weather station (MetPak™ II Remote, Gill Instruments Ltd, Lymington, Hampshire, UK). The weather station included sensors to measure wind direction and speed, air temperature, relative humidity, and barometric pressure. All measurements were performed at 1-s resolution and processed to 2-h averages for data analysis.

2.3 Data Analysis

Comparisons between the two sites initially used 1-min average mixing ratios aggregated to 2-h intervals if at least 20 % of the 1-min averages represented concurrent measurements at both sites. For each 2-h interval the following two statistical parameters were computed: (1) the average greenhouse gas mixing ratios; and (2) the quantile of the CO_2 and CH_4 frequency distribution within each 2-h interval based on 1-min data, which separates the lowest 5 % from the upper 95 % of the observed mixing ratios (referred to as the 5th percentile). Similar to the arithmetic mean or the median (= 50th percentile), the 5th percentile acts as a low-pass filter. This was necessary since the frequency distribution of CH_4 mixing ratios is positively skewed towards higher mixing ratios at the mountain-top station. In contrast, the lower tail of the frequency distribution is much less influenced by outliers, thus suggesting that the 5th percentile is more likely to represent air parcels unaffected by local sources than the arithmetic mean. One drawback of the 5th percentile, however, is its high sensitivity to local sinks (for example the biospheric sink for CO_2). Two-hourly averages and 5th percentile values were used for further analysis of the atmospheric greenhouse gas mixing ratios at the two stations.

To identify a filter criterion for the mountain-top station that eliminates unwanted local influences that do not relate to regional-scale greenhouse gas fluxes, we evaluated

differences between mountain-top and tall-tower mixing ratios using these aggregated data. We calculated binned average differences according to wind speed, wind direction and atmospheric stability at the mountain-top site (see Supplementary Material, Section S2).

To determine the level of agreement between wind-direction measurements at the two sites, we used a kernel distribution in a polar coordinate system. The kernel density estimation of wind direction was calculated using the procedure described by Botev et al. (2010). As differences in CH_4 mixing ratios between the mountain-top and the tall-tower sites may be due to local CH_4 sources at the mountain-top site, we investigated between-site differences in CH_4 mixing ratios and their dependence on wind direction observed at the mountain-top site. To this end, we grouped the differences between the corresponding 2-h tall-tower and mountain-top mixing ratios into 18 wind sectors (each spanning 20 °). Then, the average differences in CH_4 mixing ratios between the sites were calculated for daytime (0800–1600 UTC) and nighttime (2000–0400 UTC), summer (April to October) and winter (November to March) and for each wind sector. More detailed information on the aggregation of these classes is presented in the Supplementary Material (Section S3, Figs. S2 and S4). For CO_2, the same procedure was repeated using a slightly modified temporal (morning: 0800–1200 UTC, afternoon: 1200-1600 UTC, evening: 2000-2400 UTC and night: 0000-0400 UTC) and seasonal classification (spring: April to June, summer/autumn: July to October, winter: November to March) to account for the differences in sources and sinks of CO_2 in comparison with CH_4.

In order to determine the general agreement between the two sites, we used the 5th percentile time series and the time series after removing periods with unfavourable flow conditions for CO_2 and CH_4 and calculated the bias and Pearson's correlation coefficients between the tall-tower and the mountain-top stations. The bias after filtering was evaluated for different months and times of day, whereas the correlation coefficient was calculated between the filtered time series of CO_2 and CH_4 mixing ratios within time periods of ±7 days centred at each 2-h value.

3 Results

3.1 Wind Directions at the Tall-tower and the Mountain-top Site

Wind directions at the mountain-top site were similar to those at the tall-tower site (Fig. 2a, b), but with a few noteworthy differences. Wind directions at the tall-tower site were dominated by the typical south-westerly and north-easterly directions found over the Swiss Plateau due to the channelling of flow between the Alps and the Jura mountains (Wanner and Furger 1990). In contrast, the flow at the mountain-top site was generally much weaker and arriving from more variable wind directions. Strongest wind at the mountain-top site was observed from the south-easterly sector (around 150 °), most probably corresponding to foehn wind.

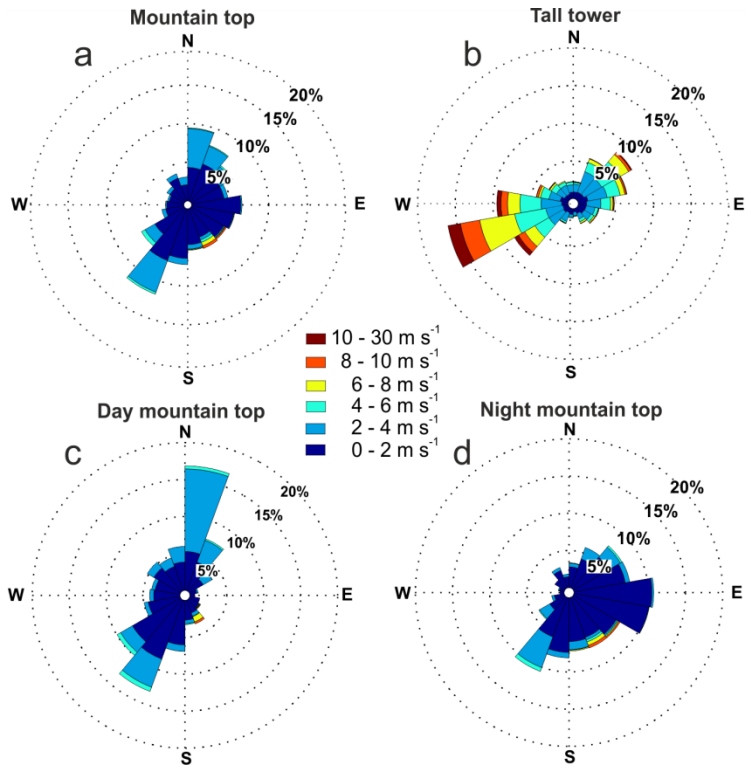

Fig. 2 Wind-rose plots for the measurement stations Früebüel (mountain top, **a**) and Beromünster (tall tower, **b**) during the year 2013 additionally separated for daytime (0800–1600 UTC, **c**) and nighttime (0000–0400 UTC, **d**) at the mountain-top station

To emphasize the influence of diurnal variations due to thermally-forced slope flow, Fig. 2c, d show wind roses at the mountain-top site separately for daytime and nighttime.

While flow from northerly directions was most frequent during daytime, nighttime flow was predominantly from southerly or easterly directions. Flow from easterly and westerly directions was generally weak, more frequently arriving from the east at night and from the west during the day.

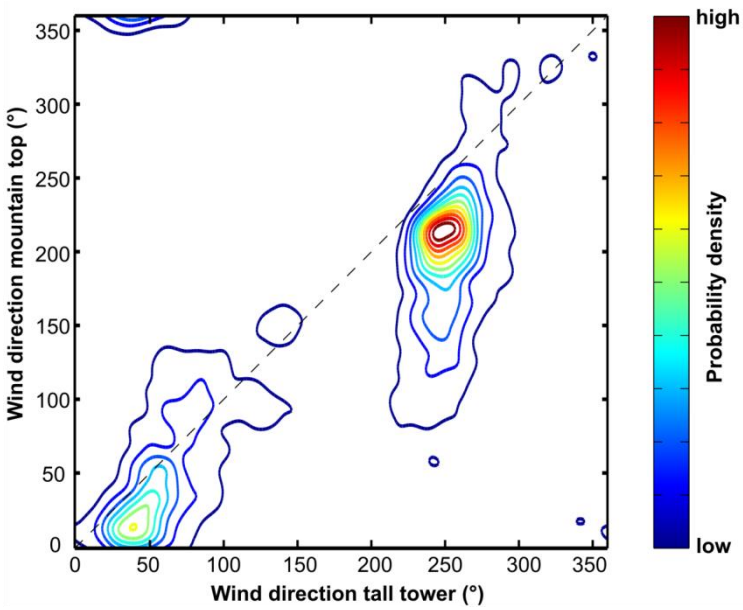

Fig. 3 Probability density distribution of wind directions at the Beromünster tall-tower station (horizontal axis) versus the Früebüel mountain-top station (vertical axis) based on a bivariate kernel density estimation. Reddish colours denote a high probability density, while bluish colours depict lower probability densities

The kernel density plot of the bivariate probability distribution between wind directions (Fig. 3) showed that flows from the north-easterly sector at the tall-tower site were accompanied by flows from a similar direction also at the mountain-top site. Larger directional spread was found at the mountain-top site, whereas the tall-tower site experienced rather well defined south-westerly flow (220 °–270 °). Under these conditions, the wind directions at Früebüel varied over a wider range of angles, but the peak of the joint probability distribution showed a relatively small directional bias (≈ 20 °–30 °), likely reflecting the influence of the surface drag at the mountain top compared to the tower measurements that are more representative of mid-boundary layer conditions.

3.2 Greenhouse Gas Variations

Methane: Despite notable differences in wind direction and wind speed between the two sites (Figs. 2 and 3), CH_4 mixing ratios followed a similar seasonal course (Fig. 4a), with mixing ratios varying roughly between 1.8 ppm and 2.2 ppm. Peak CH_4 mixing ratios observed at the mountain-top site, however, deviated by up to 0.2 ppm from mixing ratios observed at the tall-tower site. The positive outliers were most likely influenced by local CH_4 sources at the mountain-top site.

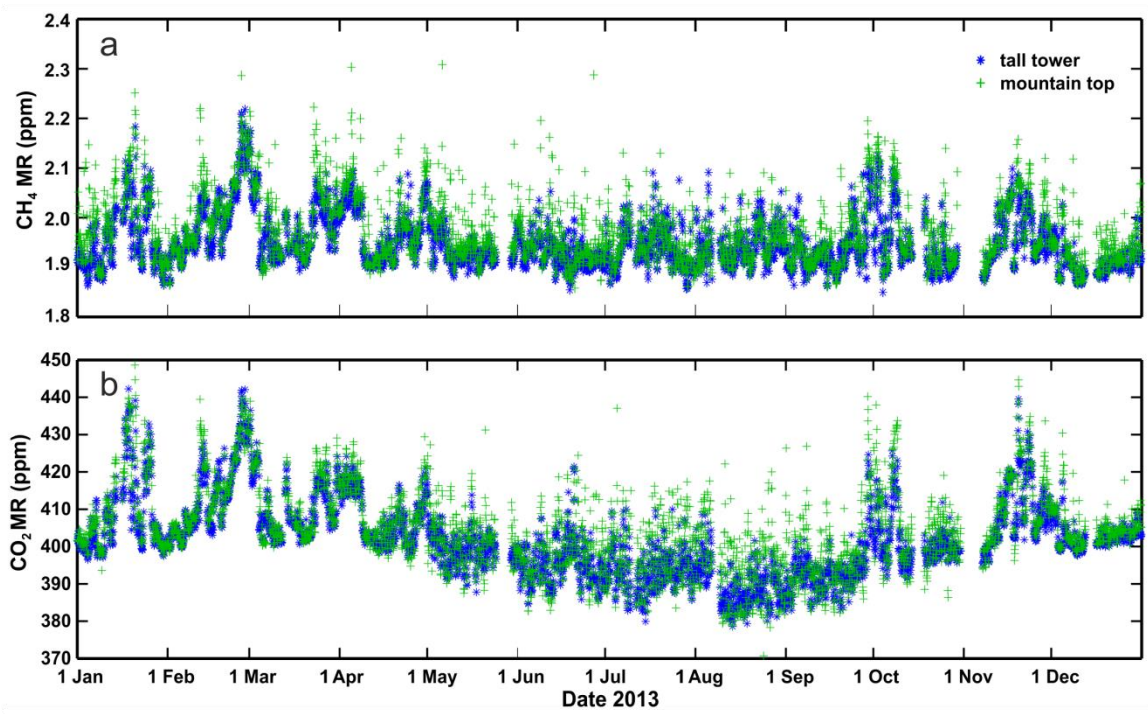

Fig. 4 Time series of 2-h averages of CH_4 (**a**), and CO_2 (**b**) mixing ratios measured at the Beromünster tall-tower station (blue symbols) compared to those measured at the Früebüel mountain-top station (green symbols) from January to December 2013

For average CH_4 mixing ratios these differences between the two stations remained generally below 0.02 ppm for any wind direction, except for southerly flow from the direction of the ETH research station when average mixing ratios at the mountain-top site were considerably higher (up to 0.065 ppm, Fig. S1 in Supplementary Material). This pattern indicates that the major source for methane at this site is the farmstead of the ETH research station.

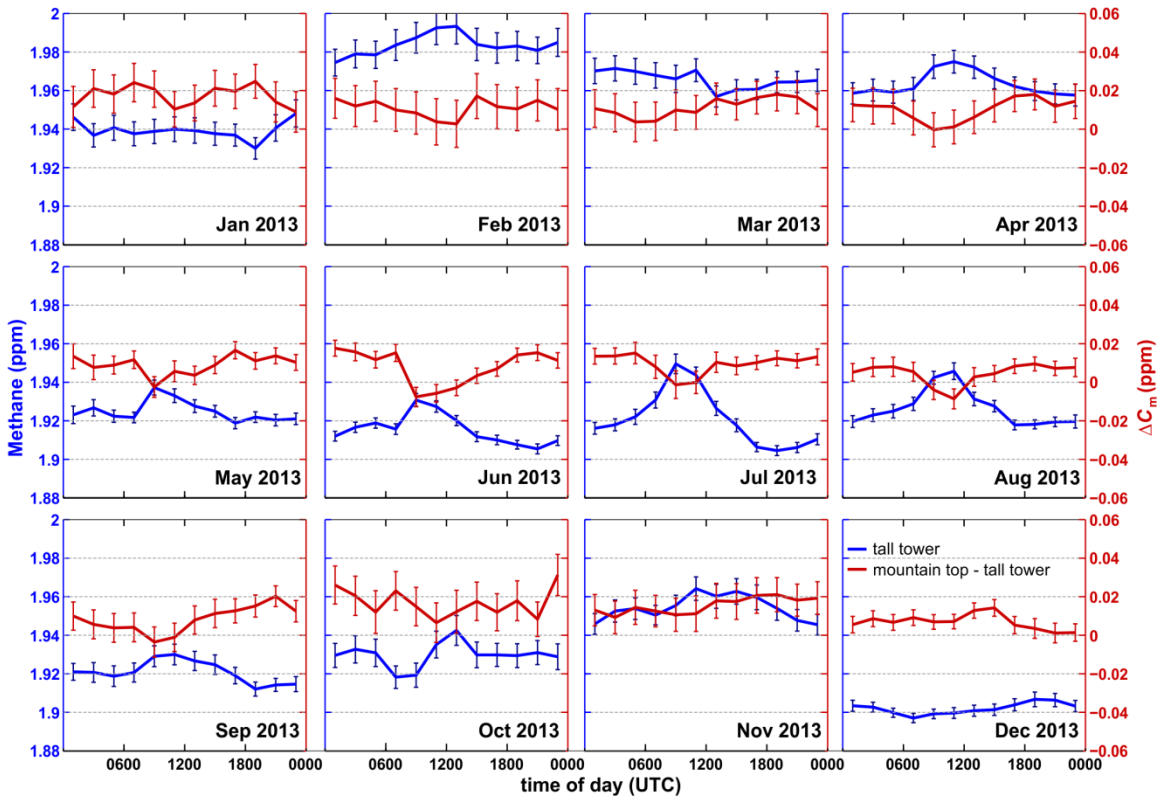

Fig. 5 Monthly average diurnal cycles derived from the 5th percentiles of the 2-h frequency distribution of CH_4 mixing ratios observed at the Beromünster tall-tower station (blue colour) and the difference in CH_4 mixing ratios between the mountain-top and the tall-tower stations (ΔC_m, red colour) including the corresponding 95% confidence interval (vertical bars) from January to December 2013

The influence of local sources was investigated by analyzing monthly aggregated diurnal patterns of the 5th percentiles of the CH_4 mixing ratios at 2-h resolution. Such CH_4 mixing ratios only showed weak diurnal patterns at the mountain top, whereas an increase of up to 0.025 ppm was seen in the late morning or around midday at the tall-tower station, especially during the summer months (Fig. 5). Except for the late morning/midday minima when methane mixing ratios at the mountain-top station were lower than at the tall-tower station, monthly averages of CH_4 mixing ratios were moderately but significantly higher at the mountain-top site (between 0.005 ppm in August and 0.020 ppm in January) than at the tall-tower site (Fig. 5, red line). A generally weak bimodal seasonal pattern of methane mixing ratios was observed. At both sites, mixing ratios were low during winter (December and January), reached their first

maximum during February, then declined slowly during the summer and exhibited a second maximum in November.

Carbon dioxide: During winter, CO_2 mixing ratios at the mountain-top and tall-tower stations almost followed the same temporal course, mostly fluctuating between 400 ppm (daytime) and 440 ppm (nighttime; Fig. 4b). In summer, however, the average CO_2 mixing ratios at the mountain top station were lower and varied between 380 ppm and 420 ppm. In general, CO_2 mixing ratios in summer were lower than in winter.

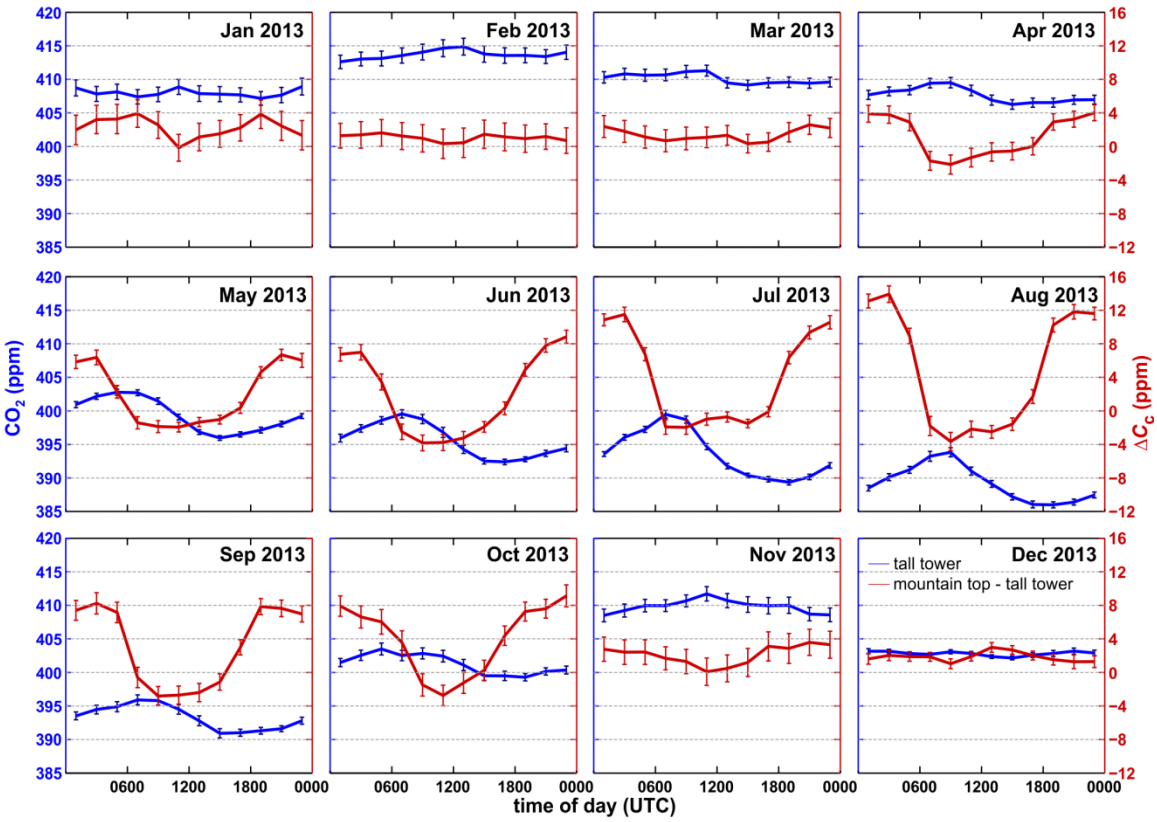

Fig. 6 Monthly average diurnal cycles of the 2-h frequency distribution of CO_2 mixing ratios observed at the Beromünster tall-tower station (blue colour) and the difference in CO_2 mixing ratios between the tall-tower and the mountain-top stations (ΔC_c, red colour) including the corresponding 95% confidence interval (vertical bars) from January to December 2013

To investigate the difference in summertime CO_2 mixing ratios between the two sites, average diurnal cycles of CO_2 for each month and both stations were calculated in an analogous manner to CH_4, but using averages instead of 5th percentiles (since the 5th

percentile approach did not work satisfactorily for CO_2) (Fig. 6). During wintertime, only a weak diurnal cycle of CO_2 mixing ratios could be seen at the tall-tower station, showing a slight increase of up to 4 ppm during midday. This increase in midday CO_2 mixing ratios was not observed at the mountain-top station and thus the bias between the mountain-top and the tall-tower stations (red line in Fig. 6) usually decreased around this time of day. CO_2 mixing ratios always remained close to 410 ppm (except during December when CO_2 mixing ratios approached 400 ppm). In summer, CO_2 mixing ratios at the mountain-top site showed a typical diurnal cycle with lowest values during daytime and a maximum at night. Summertime CO_2 mixing ratios at the tall-tower site had their maximum in the morning and reached lowest values in the afternoon. Thus, the bias in CO_2 mixing ratios was usually negative during the day and positive at nighttime.

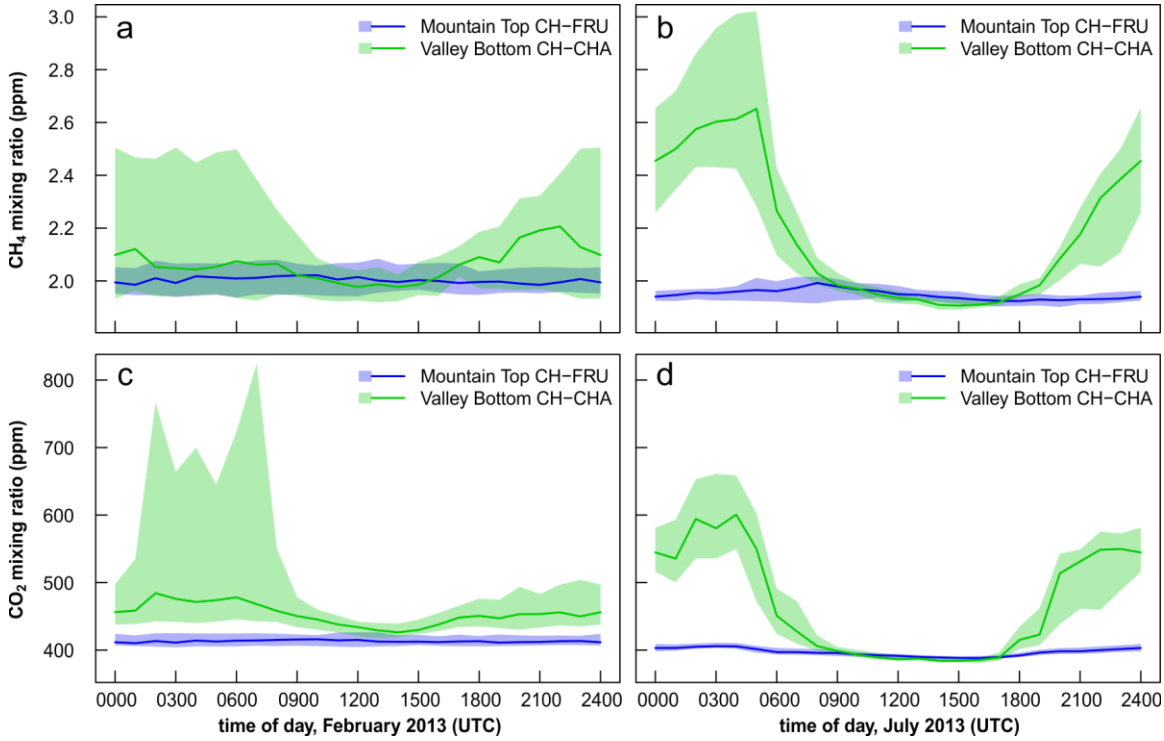

Fig. 7 Diurnal cycles of median CH_4 (**a**, **b**) and CO_2 (**c**, **d**) mixing ratios at the mountain-top station (Früebüel CH–FRU, blue colour) and a nearby valley-bottom station at 393 m a.s.l. (Chamau CH–CHA 47°12′37″N, 8°24′38″E, green colour; Merbold et al. 2014) for a representative month in the winter (February 2013, **a**, **c**) and summer (July 2013, **b**, **d**). The green and blue shaded areas indicate the interquartile range for the valley bottom and mountain-top station, respectively

Near-surface CH_4 mixing ratios at the mountain-top site showed a less distinct diurnal cycle than at a nearby (ca. 15 km distance) valley-bottom site (Chamau, cf. Fig.7), where nighttime CH_4 mixing ratios increased up to 2.4 ppm and 2.2 ppm in July and February, respectively. These valley-bottom data were collected and published by Merbold et al. (2014) and are only shown for comparison. A similar difference between mountain-top and valley-bottom sites is seen in CO_2 mixing ratios, with a very weak nighttime increase of approximately 20 ppm at the mountain-top site in July 2013 as compared to the 200-ppm increase observed at the valley-bottom site.

3.3. Filtering CH_4 and CO_2 and Mixing Ratio Differences to Minimize Local Influences

The percentile filtering approach revealed to be highly capable of removing a relevant share of mixing ratios influenced by local sources, but is not based on physical considerations, since it only uses a statistical filtering criterion. Hence, we also applied a second filtering approach that employs meteorological information. With this second approach, wind speeds and wind directions could be identified that led to large differences between mountain-top and tall-tower measurements. These were then discarded. From the retained subset of measurements, the signal with minimal influence of local conditions was extracted as a function of time of day and season. An analysis of variance approach was used to determine the aggregation levels for wind speed, wind direction, time of day, and seasonality. The aggregation levels differed slightly for CH_4 and CO_2 mixing ratios. Details are given in Supplementary Material, Sections S3.1 and S3.2. For simplicity, we termed this meteorological filtering the “WDS filter” (W for wind speed and direction, D for time of day, and S for seasonality).

The differences of CH_4 mixing ratios between the mountain-top and the tall-tower sites (ΔC_m) were best explained by the four factors: wind direction (three classes), wind speed (five classes), time of day (separated into daytime 0800–1600 UTC and nighttime 0000–0400 UTC), and seasonality (two classes: summer, April to October; and winter, November to March). For CO_2, the between-site difference of mixing ratios (ΔC_c) depended on the same four factors but required a higher degree of detail, with four classes for time of day (morning: 0800–1200 UTC, afternoon: 1200–1600, evening:

2000–2400 UTC, and night: 0000–0400 UTC) and three classes for season (spring: April to June, summer/autumn: July to October, and winter: November to March). Transition periods between night and morning (0400–0800 UTC) and between afternoon and evening (1600–2000 UTC) were excluded from this analysis since during these time periods conditions are changing rapidly and may result in mixing ratios that are representative of neither daytime nor of nighttime conditions. This classification was coarse enough to be meaningful but still detailed enough to represent the pronounced diurnal cycle of the CO_2 mixing ratios (Fig. 6).

Before applying such a filter, a clear dependence of ΔC_m and ΔC_c mixing ratio differences on all four factors was obvious (Figs. 8 and 9). Wind direction had a comparatively larger influence on ΔC_m (Fig. 8) than ΔC_c (Fig. 9).

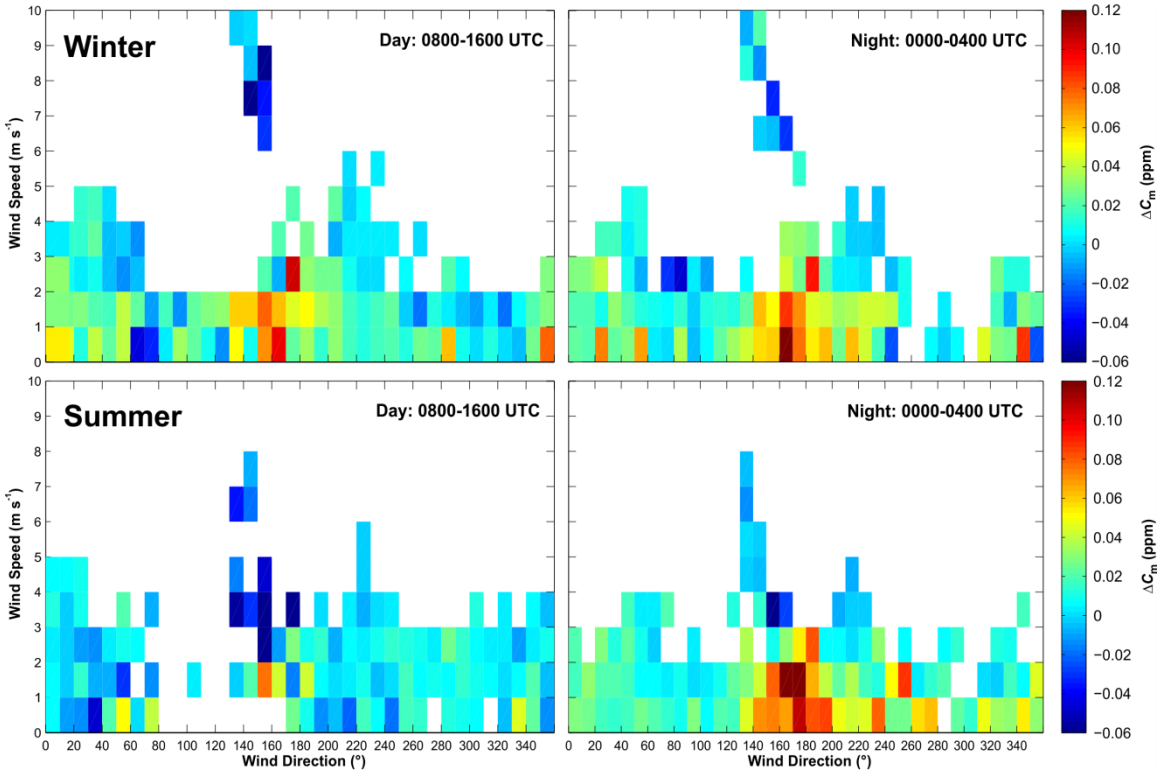

Fig. 8 Average differences of daytime (0800–1600 UTC, left) and nighttime (0000–0400 UTC, right) CH_4 mixing ratios between mountain-top and tall-tower station (ΔC_m) during the winter season (November–March, top) and the summer season (April–October, bottom), binned for different wind direction and wind speed classes at the mountain top

Under strong (> 3 m s^{-1}) south-easterly flow (130 ° to 170 °), CH_4 mixing ratios tended to be up to 0.06 ppm lower at the mountain-top site compared to the tall-tower site, especially during daytime (Fig. 8). In contrast, CH_4 mixing ratios were up to 0.07 ppm higher at the mountain-top site compared to the tall-tower site with wind speeds < 3 m s^{-1} and wind directions from 120 ° to 200 ° corresponding to the sectors influenced by the ETH farmstead (Fig. S1). Negative ΔC_m mixing ratio differences were also observed during easterly flow (60 °–120 °) with wind speeds > 2 m s^{-1}. Especially in summer, positive deviations of the mountain-top from the tall-tower measurements tended to be higher during the night than during the day.

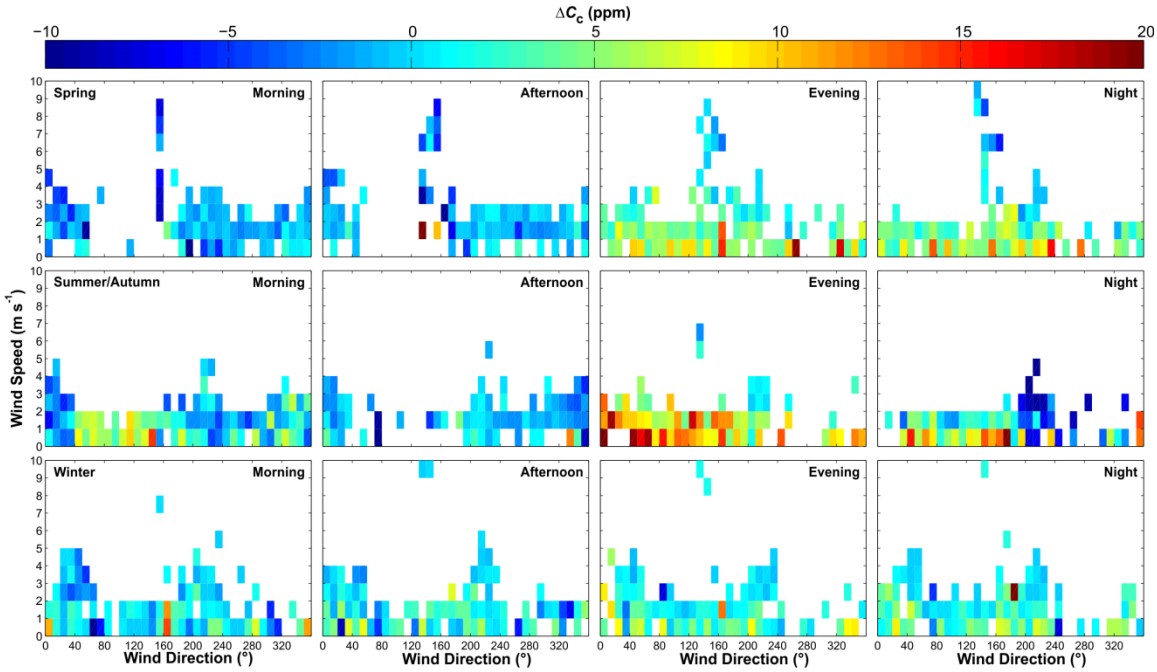

Fig. 9 Average differences of morning (0800–1200 UTC, left), afternoon (1200–1600 UTC), evening (2000–2400 UTC), and night (0000–0400 UTC) CO_2 mixing ratios between mountain-top and tall-tower station (ΔC_c) during spring (April-June, top), summer/autumn (July-October, centre) and the winter season (November-March, bottom) binned for different wind direction and wind speed classes at the mountain top

The weak wind direction dependency of ΔC_c (Fig. 9) compared to ΔC_m (Fig. 8) is not surprising because the main local source and sink for CO_2 at the mountain top is the vegetation which extends around the measurement station in all directions. During spring, daytime CO_2 mixing ratios (morning, afternoon) at the mountain-top station were

generally lower than at the tall-tower station, irrespective of wind direction. Contrastingly, CO_2 mixing ratios measured during evening and night were increased at the mountain-top station as compared to the tall-tower station. Similar conditions were found in summer/autumn except with easterly wind directions in the morning ($\Delta C_c > 0$ ppm) and with south-westerly wind directions during the night ($\Delta C_c < 0$ ppm). In winter, ΔC_c was generally smaller than in summer, and wind directions 90 °–160 ° and 190 °–260 ° tended to show the smallest differences between the mountain-top and the tall-tower measurements (Fig. 9).

3.4 Comparison of Greenhouse Gas Mixing Ratios

All wind directions with strong local influence on CH_4 or CO_2 mixing ratios were filtered out based on the analysis of variance results shown in Supplementary Material (Tables S2 and S3). CH_4 mixing ratios were maintained if the following conditions were met: (1) summer daytime wind directions in the range 0 °–50 ° or 190 °–360 °, (2) summer nighttime wind directions in the range 10 °–120 ° or 200 °–360 ° in combination with wind speeds > 2 m s^{-1}, (3) winter daytime wind directions in the range 0 °–70 ° combined with wind speeds > 2 m s^{-1}, (4) winter daytime wind directions in the range 220 °–360 ° combined with wind speeds > 1 m s^{-1}, (5) winter nighttime wind speeds in the range 1–2 m s^{-1} and wind directions in the range 40 °–130 °, and (6) winter nighttime wind directions in the range 200 °–260 ° and wind speeds > 2 m s^{-1}. The remaining CH_4 mixing ratios were used for further analysis.

CO_2 mixing ratios at the mountain-top station during spring or autumn were generally either higher or lower than at the tall-tower station, thus filtering of CO_2 mixing ratios was problematic: In winter only CO_2 mixing ratios could be retained when wind direction was 90 °–160 ° or 190 °–260 ° in combination with wind speeds > 1 m s^{-1} irrespective of time of day. In summer, all CO_2 mixing ratios at the mountain-top station were strongly affected by CO_2 uptake (photosynthesis) by vegetation during daytime and CO_2 release (respiration) during the night. With this data screening, 35 % of the CH_4 mixing ratios and 9 % of the CO_2 mixing ratios measured at the mountain-top station could be retained (Fig. 10 a, c).

Table 1 Average differences between the CH_4 (ΔC_m) and CO_2 (ΔC_c) mixing ratios at the mountain-top and the tall-tower station after the application of the WDS filter

	average ΔC_m mixing ratio difference ± standard deviation ΔC_m (ppm)			
	Night	**Morning**	**Afternoon**	**Evening**
January	–0.0018 ± 0.0026	0.0392 ± 0.0041	0.0252 ± 0.0025	0.0030 ± 0.0017
February	0.0041 ± 0.0009	0.0008 ± 0.0024	0.0038 ± 0.0023	0.0121 ± 0.0016
March	0.0077 ± 0.0015	0.0030 ± 0.0033	0.0135 ± 0.0018	0.0144 ± 0.0019
April	0.0074 ± 0.0013	–0.0050 ± 0.0018	0.0084 ± 0.0011	0.0167 ± 0.0016
May	0.0083 ± 0.0013	0.0082 ± 0.0016	0.0157 ± 0.0013	0.0296 ± 0.0028
June	0.0319 ± 0.0030	–0.0019 ± 0.0018	0.0043 ± 0.0013	0.0348 ± 0.0035
July	0.0091 ± 0.0018	–0.0052 ± 0.0026	0.0113 ± 0.0017	0.0071 ± 0.0010
August	–0.0018 ± 0.0010	–0.0149 ± 0.0022	0.0033 ± 0.0019	0.0047 ± 0.0012
September	–0.0005 ± 0.0010	–0.0080 ± 0.0021	0.0115 ± 0.0030	0.0156 ± 0.0028
October	0.0110 ± 0.0038	0.0141 ± 0.0034	0.0151 ± 0.0031	0.0262 ± 0.0044
November	0.0037 ± 0.0008	–0.0040 ± 0.0025	0.0145 ± 0.0016	0.0157 ± 0.0020
December	0.0106 ± 0.0022	0.0031 ± 0.0020	0.0079 ± 0.0019	–0.0007 ± 0.0014
	average ΔC_c mixing ratio difference ± standard deviation ΔC_c (ppm)			
	Night	**Morning**	**Afternoon**	**Evening**
January	1.01 ± 0.27	0.26 ± 0.18	1.99 ± 0.34	0.91 ± 0.25
February	-0.71 ± 0.21	−0.19 ± 0.19	0.11 ± 0.18	−0.27 ± 0.18
March	1.00 ± 0.18	2.84 ± 0.60	2.82 ± 0.73	2.35 ± 0.36
November	1.76 ± 0.26	1.69 ± 0.45	2.19 ± 0.64	1.34 ± 0.22
December	1.32 ± 0.24	1.05 ± 0.15	2.41 ± 0.26	0.65 ± 0.13

ΔC_m, ΔC_c: Difference in CH_4 and CO_2 mixing ratios between the mountain-top and the tall-tower station derived as average value of each 2-h bias passing the WDS filter within the corresponding time period (including the corresponding standard deviation). Night: 0000-0400 UTC; morning: 0800–1200 UTC; afternoon: 1200–1600 UTC; evening: 2000–2400 UTC. The WDS filter is a meteorological conditional filter described in Section 3.3.

These retained data are thought to best represent the regional atmospheric signal in a way that allows for a direct comparison of the mountain-top mixing ratios with those concurrently measured at the tall-tower station. Average ΔC_m after WDS filtering (Table 1) varied between –0.0149 ± 0.0022 ppm (0800–1200 UTC in August) and 0.0392 ± 0.0041 ppm (0800–1200 UTC in January). In September between 0000 and 0400 UTC, the average ΔC_m bias was closest to zero (−0.0005±0.0010 ppm). During the

morning hours, the average ΔC_m was often negative (tall-tower station observed higher values than the mountain-top station), especially in summer. Average ΔC_c after filtering varied between –0.71 ± 0.21 ppm (0000–0400 UTC in February) and 2.84 ± 0.60 ppm (0800–1200 UTC in March) and was 0.11 ± 0.18 ppm (1200–1600 UTC in February) in the best case.

In addition to the bias calculations we also performed a correlation analysis with (a) the WDS filtered 2-h mixing ratio averages and (b) the 5th percentiles of CH_4 and CO_2 mixing ratios measured at both sites. Fourteen-day running Pearson's correlation coefficients for CH_4 mixing ratios filtered with the 5th percentile exceeded $R = 0.7$ in 67 % of all cases. This means that in the majority of cases more than ≈ 50 % (derived from $R^2 \geq 0.7^2$) of the variance in the CH_4 mixing ratios at the mountain top could be explained by the concurrent tall-tower measurements and vice versa.

The WDS filter leaded to similarly high correlations between the mountain-top and the tall-tower station CH_4 mixing ratios ($R \geq 0.7$ in 67 % of the cases) as the 5th percentile (Fig. 10 b). Weaker correlations ($R < 0.7$) could often be attributed to periods with weakly varying atmospheric CH_4 mixing ratios at both stations. Usually periods with very high correlations were also characterised by offsets between the stations being close to zero. The good overall agreement between both filtered time series indicates that CH_4 mixing ratios at the mountain-top station follow the same seasonal trend as CH_4 mixing ratios at the tall-tower station, but it was not possible to completely eliminate the offset at the mountain-top station imposed by local sources and/or mountain flows, even after screening 2-h averages with a WDS filter or filtering the CH_4 data using the 5th percentile approach.

Wintertime CO_2 mixing ratios at the two stations agreed rather well after applying the 5th percentile or the WDS filter, as is indicated by the high correlation coefficients (typically $R > 0.7$). From January to April, there was an excellent agreement of CO_2 mixing ratios between the tall-tower and the mountain-top station (Fig. 10 c, d). During the growing season, the relationship was weakest (usually with $0.3 < R < 0.6$, Fig. 10 d). During winter the relationship between 5th percentiles of the CO_2 mixing ratios measured at both

stations was as good as the relationship between the WDS filtered 2-h average mixing ratios, whereas in summer the WDS filtering usually did not retain any values.

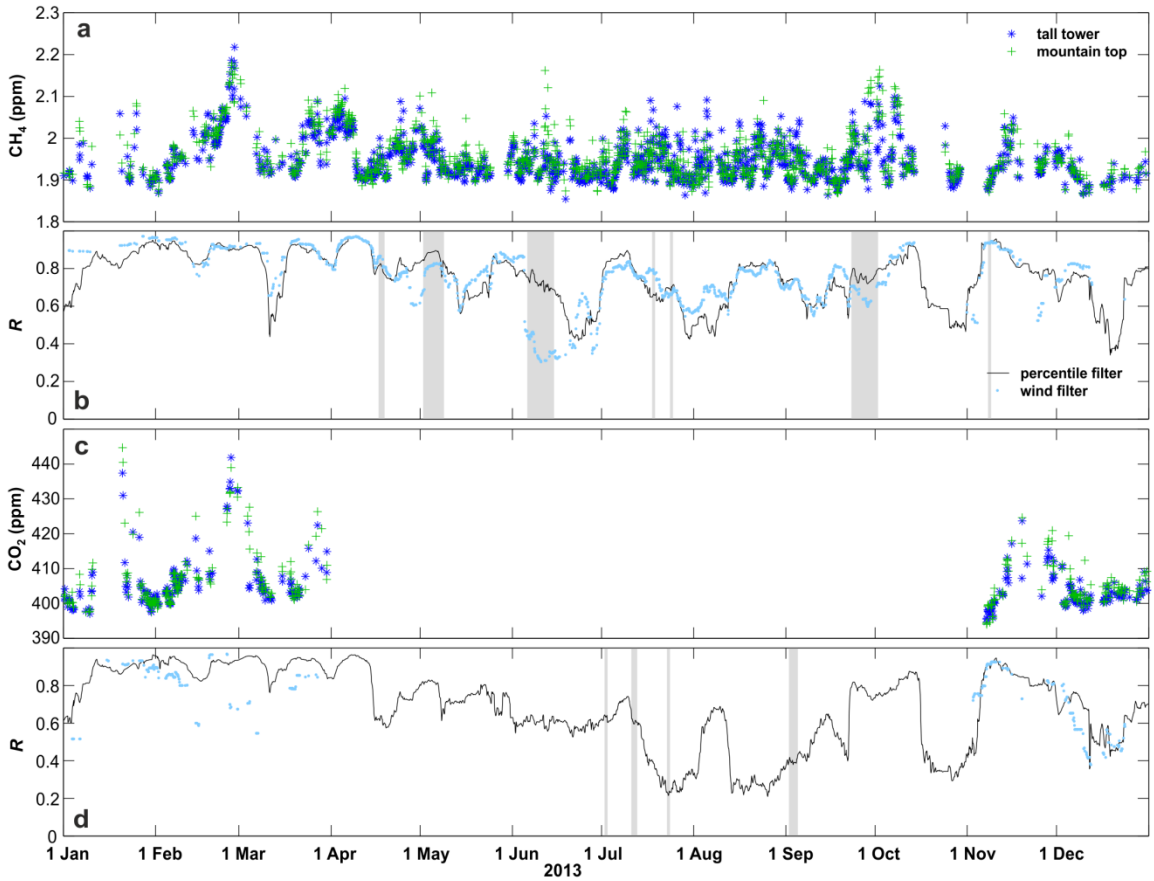

Fig. 10 Comparison of the CH_4 (**a**) and CO_2 (**c**) mixing ratios at the mountain-top (green crosses) and the tall-tower (blue asterisk) station after the application of the WDS filter. Pearson's correlation coefficients (*R*) between 5th percentiles of mountain-top and tall-tower measurements (black solid line) and 2-h averages of mountain-top and tall-tower measurements retained after WDS filtering (blue dots) calculated within a time window of ± 7 days around every measurement point are shown for CH_4 (**b**) and CO_2 (**d**), respectively. The Pearson correlation coefficients are all significantly different from zero ($p < 0.01$). Management activities affecting the surrounding meadows are highlighted in grey in panels b and d. The management activities at the mountain-top station were: application of organic fertilizer or grazing of cattle on the pastures surrounding the measurements (**b**) and harvests (**d**).

4 Discussion

Precise measurements of CO_2 and CH_4 mixing ratios have been carried out at several stations in Europe and North America already (e.g. Thompson et al. 2009, Göckede et al. 2010, Sun et al. 2010, Winderlich et al. 2010, Vermeulen et al. 2011, Lavaux et al. 2012, Miles et al. 2012, Andrews et al. 2014). To the best of our knowledge, however, this study is the first to discuss the measurements obtained at two stations in a paired-site approach, comparing a tall-tower with a neighbouring (≈ 28 km separation) mountain-top station at a similar elevation above sea level. Since local effects are usually not represented well in atmospheric transport models it is essential to extract the regional signal from mountain-top measurements. Thus, the key challenge for inverse modelling in the comparison between tall-tower and mountain-top greenhouse gas mixing ratios is the filtering of the dataset to remove local influences that only affect one but not the other site. On the other hand, meteorologists trying to qualitatively and quantitatively understand such local effects in complex terrain are typically interested in periods or in meteorological conditions when differences between two sites are largest. In order to address both aspects, we first discuss the extraction of the regional signal using the filtering approach suggested in Section 3.3, and then address the meteorological differences between the sites under conditions when local effects play an important role.

4.1 Extracting the Regional Signal

Two approaches were used to extract the regional signal from the time series of mixing ratio measurements: (i) using a statistical percentile filter, and (ii) using a conditional filter based on wind direction, wind speed, time of day, and season (WDS filter). An alternative filtering approach, which was already used to screen data from well mixed air masses, is time-of-day filtering (Göckede et al. 2010, Peters et al. 2010), which exclusively uses well mixed afternoon conditions and nighttime measurements in the residual layer well above the nocturnal boundary layer. More sophisticated statistical approaches which have been used to filter mountain-top measurements are (i) short-term variance filters and (ii) weighted median smoothers (Brooks et al., 2012). In our case, the 5th percentile approach proved to be a suitable choice to filter outliers related to local CH_4 sources. However, this approach makes the implicit assumption that within a 2-hour time

period the lower-than-average mixing ratios are most likely closest to the regional signal, while higher-than-average mixing ratios are more likely to be outliers caused by local sources. Using a 5th percentile filter led to rather robust comparisons between tall-tower and mountain-top sites for CH_4 mixing ratios (Fig. 5). Its shortcomings, however, are its relatively strong sensitivity to local sinks, its statistical and non-causal basis, and the fact that there is no clear threshold that would establish the 5th percentile as the best choice everywhere. Contrastingly, the second approach – the WDS filter – uses conditional criteria that are easier to understand in the context of impacts of the local topography and local surface fluxes. For CH_4, both filtering approaches seem to be useful, whereas in the case of CO_2 none of the filters worked well during the growing season (Fig. 10), indicating that the regional signal is too strongly altered by local influences to be extracted with a WDS filter.

4.2 The Importance of Local Effects

4.2.1 Terrain Driven Effects on Greenhouse Gas Mixing Ratios

The accumulation of CH_4 and other trace gases in the nocturnal boundary layer at valley-bottom sites during the night is a general pattern found in diurnal cycles of mixing ratio measurements and has been used before to determine regional-scale CH_4 fluxes (e.g., Stieger et al. 2015). At the mountain top, cold air drainage flows prevent the build-up of a deep, stable nocturnal boundary layer and thus the boundary layer extends 200–300 m above the valley bottom, even in broad valleys such as the Swiss Plateau (cf. Eugster and Siegrist, 2000; see also Stieger et al., 2015). Hence, although our mountain-top measurements were only performed at 4-m height above ground surface, the diurnal courses of CH_4 and CO_2 mixing ratios rather followed that of the tall-tower site (Figs. 5 and 6) than that of a valley-bottom site (Fig. 7). This indicates that the mountain-top station – similarly to the tall-tower station – remains above the stable nocturnal boundary layer of the surrounding valleys, where agriculturally driven methane emissions lead to a substantial increase of methane during the night (Fig. 7). Consequently, both sites were decoupled from the conditions at the valley floor during the night. This agrees well with mobile measurements that were performed along the slopes of the Reuss valley and up to

the Früebüel mountain-top site (Bamberger et al. 2014) which clearly showed that the nocturnal boundary-layer depth is only between 100 m and 200 m deep during clear summer days, while the Früebüel mountain-top site is located almost 500 m above the valley floor. Considering the low sampling height above ground, however, the mountain-top site is located in the local surface layer.

Greenhouse gas mixing ratios at the tall-tower site showed a well-known increase of mixing ratios in the late morning with the onset of daytime convective mixing (Davis et al. 2003) which was virtually absent at the mountain-top site. The absence of the late morning peak at the mountain top can be explained by its location on top of a mountain ridge on the easterly side of the Reuss valley (Bamberger et al. 2014). The onset of daytime convective mixing and vertical advection of nighttime pollution along the warmer hillslopes is a pattern that is common to mountainous regions (Gohm et al. 2009, Schnitzhofer et al. 2014). Considering the diurnal cycle of greenhouse gas mixing ratios, the tall-tower station (nominally 212 m a.g.l.) also profits from its position on a local hill that removes the tower top from the valley bottom (where CH_4 and CO_2 accumulates during the night) by an additional ≈ 300 m: the tower base is at 797 m a.s.l., whereas the flat areas surrounding the locality are at 463 m (Lake Baldegg) to 504 m a.s.l. (Lake Sempach). Without this additional topographic height, more pronounced diurnal cycles in CH_4 and CO_2 mixing ratios would be expected at the tall-tower site: Winderlich et al. (2014) found that at the highest level (301 m above ground) of the Zotino tower, Siberia, occasional nocturnal increases in CH_4 mixing ratios occur.

All these considerations suggest that for both mountain-top and tall-tower sites it is not the height of a measurement from the local ground that matters, but the larger-scale topographic context, and thus the altitude above the topographic reference elevation, which is typically the bottom of a larger and broader valley where nocturnal accumulation of greenhouse gases takes place.

4.2.2 Effects of Local Flow

Flows at the tall-tower and the mountain-top stations showed both a strong channelling along the two main wind directions (north-east and south-west) and minor contributions from other directions, mostly in combination with low wind speeds. On the other hand,

there was a directional shift between the main wind directions at the mountain-top site (which was turned anti-clockwise) as compared with the tall-tower site. However, such a rotation of the flow between the surface and the mid-boundary layer is well known as the Ekman spiral (e.g. Holton 2004). Due to the well-known natural increase of wind speed with height above surface, wind speeds within the surface layer measured at 2 m a.g.l. at the mountain-top site were considerably lower than those at the tall-tower site (at 212 m a.g.l.) In addition, wind speeds at the tall-tower site were maximal during the night, whereas they were lowest during the night at the mountain-top site, at least during summer (Oney et al. 2015).

At the mountain top, flow from south-easterly direction was occasionally stronger (up to 10 m s^{-1}) than flow from other directions. These high wind speeds usually occurred in combination with high temperatures and persistent wind directions (data not shown) and indicated the influence of foehn winds (warm and dry southerly winds across the Alps). The influence of foehn winds at the mountain-top station is plausible as it is located near the main axis of the Reuss Valley, one of the main foehn valleys in Switzerland (Seibert 1990), whereas the tall-tower station is much more sheltered against the southerly flow by Mount Rigi and other mountain ridges and is further away from the Alps. At the mountain-top station, wind directions outside the usual easterly or westerly directions were more frequent than at the tall-tower station but generally weak (mostly < 2 m s^{-1}), suggesting thermally induced south-westerly flows along the slopes of the Zugerberg mountain ridge and larger scale northerly plain-to-mountain flows (Lugauer and Winkler 2005), a phenomenon commonly referred to as Alpine pumping. While easterly (down-slope) winds were seen predominantly during night-time, westerly (up-slope) winds were more frequent during the day, agreeing with the typical picture of diurnal mountain winds (Whiteman 2000) in the surface layer. These findings agree with the findings by Oney et al. (2015) that the local environment influences prevailing wind directions more at the mountain-top station than at the tall-tower station.

4.2.3 The Effect of Local Sources and Sinks

During time periods when the ETH research station and its farmstead buildings were in upwind direction of the mountain-top site the offset between both stations was 0.065 ppm

on average, whereas it was much lower (< 0.01 ppm) for all other wind directions (see Fig. S1). The small directional deviation between the sector with highest CH_4 mixing ratios and the farmstead buildings (seen in Fig. S1) relates to the influence of local terrain. The close farmstead obviously acted as a source of CH_4 which considerably influenced the mixing ratios when the flow came from that direction (Figs. S1 and 8). With higher wind speeds and south-easterly flow, CH_4 and CO_2 mixing ratios at the mountain-top site were typically lower than those at the tall-tower site (Figs. 8 and 9). This indicates that the mountain-top station observes relatively clean free-tropospheric air masses descending in the lee of the Alps during foehn as opposed to the tall-tower station measuring planetary boundary-layer air. Since foehn wind tends to follow the terrain similarly to hydraulic flows, our assumption that the same elevation above sea level can be compared fails under such special conditions where altitude above the topographic reference surface becomes more relevant than the absolute elevation. Additionally, during nighttime and in winter, when vertical mixing is generally weaker, mixing ratios at wind speeds < 2 m s^{-1} were often larger at the mountain-top as compared to the tall-tower station, especially with westerly up-slope winds and northerly winds which most likely originated from lower parts of the valley. Thus, with the WDS filter all conditions with (a) flow from the farmstead, (b) wind directions and speeds associated with foehn, and (c) during times with reduced vertical mixing, wind speeds < 2 m s^{-1} and northerly or westerly wind directions were removed from the time series. When wind speeds are low (0–1 m s^{-1}), wind directions are often not properly defined or very variable. This could explain why CH_4 mixing ratios at wind speeds < 1 m s^{-1} are higher at the mountain top even if wind direction does not include the local farmstead. Moreover, a strong northerly or westerly component in the flow means that the air mass passed the Zugerberg mountain ridge where other farmsteads are located. During periods of low solar radiation, weak turbulence, and low wind speeds, the influences from more remote farmsteads could be increased, which could explain the higher CH_4 mixing ratios observed at the mountain-top station.

Periods when CO_2 mixing ratios were higher at the mountain-top station than those at the tall-tower site did not show such pronounced wind-direction dependence as did CH_4. In spring and summer/autumn, the difference between CO_2 mixing ratios at the mountain-

top and the tall-tower station was typically highest with lower wind speeds < 2 m s^{-1} and reduced vertical mixing (evening, night). As the vegetation surrounding the mountain-top site is covered by grassland and forests, it acted both as a source (respiration) and a strong sink (photosynthesis) of CO_2 depending on time of day or season and management (Zeeman et al. 2010). This generally limited the capability to distil the anthropogenic CO_2 signal out of the CO_2 mixing ratio time series. Here an increased measurement height above the local surface may help to reduce the strong influence from the vegetation (e.g. Bakwin et al. 1995, 1998). Alternatively, there are methods to estimate regional fluxes based on vertical gradients of mixing ratios between the atmospheric boundary layer and the free troposphere at tower sites (e.g. Bakwin et al. 2004, Crevoisier et al. 2006). In a well-mixed atmospheric boundary layer, flux–gradient relationships (Monin and Obukhov 1954, Moeng and Wyngaard 1984, 1989) have been used to adjust for biases introduced by low measurement heights (Bakwin et al. 2004). In winter, CO_2 mixing ratios at the mountain-top were often higher than at the tall-tower site with flows from the farmstead and flows from northerly or westerly directions, similarly to CH_4 mixing ratios. These high biases were most frequent during periods of reduced vertical mixing and thus were removed from our analysis.

In summary, our comparison between a tall-tower site and a mountain-top site provided evidence that the regional signal of CH_4 mixing ratios can be extracted from the time series even under the presence of geographically constrained local sources. However, a bias of approximately 0.01 ppm in the CH_4 mixing ratio has to be taken into account. It remains much more challenging to do the same with CO_2 mixing ratios due to the dominance of the local biogenic signal present in the measurements when plant photosynthesis and ecosystem respiration are most active.

5 Conclusions

Atmospheric CO_2 and CH_4 observations at a mountain-top site have been compared to measurements at a neighbouring tall-tower site (within 28.4 km horizontal distance) at a similar elevation above sea level. Although the airflow was significantly perturbed locally at the mountain-top site, CH_4 mixing ratios were quite similar to those at the tall-

tower site, except for peak values. Average mountain-top and tall-tower CH_4 mixing ratios showed good agreement, with an average CH_4 bias between the two stations that was around 0.01 ppm, after applying a filter to select for favorable wind direction, wind speeds, time of day and season at the mountain-top site, and 5th percentiles of the 2-h frequency distribution of CH_4 mixing ratios at both sites. Peak mixing ratios of unfiltered data, however, were clearly influenced more by local CH_4 sources at the mountain top site than at the tall-tower site. Consequently, it was possible to minimize, but not to completely remove, the influence of local agricultural CH_4 sources by choosing an appropriate filter. Hence, we conclude that, at least in absence of local sources, a mountain-top station can provide greenhouse gas observations with similar regional representativeness as a tall-tower station. Geographically well-defined CH_4 sources may be acceptable to a certain degree as their influence can be removed with appropriate filtering. However, it is generally preferable to choose the location of mountain-top sites in a way that local sources are virtually absent.

For CO_2, however, the usefulness of mountain-top mixing ratio measurements may be more limited for inverse modelling, especially during summer, when vegetation and soils cause a more pronounced diurnal cycle at the mountain top than on the top of a tall tower. Since these diurnal and seasonal signals are strong, a filter based on local wind conditions, time of day, and season is not able to remove all local influences of the vegetation at the mountain-top site. At sites where the larger-scale (far-field) signal to local-scale noise ratio remains an issue, an increased measurement height should be considered, leading to a dilution and damping of the local-scale noise. Being aware of such limitations, we conclude that a carefully selected mountain-top site still can be considered a suitable alternative for a tall-tower station. Mountain sites have a similar potential for continuous long-term monitoring, and could complement tall-tower stations, especially in mountainous terrain.

Acknowledgements The study was financially supported by the Swiss National Science Foundation under the grant number CRSII2_136273. The authors acknowledge the staff members of the ETH research station for the agricultural management at the mountain-top site and the technicians of the ETH Grassland Sciences Group, Peter Plüss and Thomas Baur, for their assistance during installation and setup of the measurement station at Früebüel. We acknowledge the tower-site installation at Beromünster designed by

Rüdiger Schanda, Peter Nyfeler, Hanspeter Moret, Samuel Marending from the University of Bern and installed by Cablex AG (Bern, Switzerland). Further, the authors acknowledge Swisscom for granting access to the tall tower, and the local authorities for the construction permit. Susanne Burri, Carmen Emmel, Anna Gilgen, Lukas Hörtnagl and Lutz Merbold from the Grassland Sciences Group are acknowledged for their helpful scientific discussions.

References

Andrews AE, Kofler JD, Trudeau ME, Williams JC, Neff DH, Masarie KA, Chao DY, Kitzis DR, Novelli PC, Zhao CL, Dlugokencky EJ, Lang PM, Crotwell MJ, Fischer ML, Parker MJ, Lee JT, Baumann DD, Desai AR, Stanier CO, De Wekker SFJ, Wolfe DE, Munger JW, Tans PP (2014) CO_2, CO, and CH_4 measurements from tall towers in the NOAA Earth System Research Laboratory's Global Greenhouse Gas Reference Network: instrumentation, uncertainty analysis, and recommendations for future high-accuracy greenhouse gas monitoring efforts. Atmos Meas Tech 7:647–687. doi: 10.5194/amt-7-647-2014

Bakwin PS, Davis KJ, YI C, Wofsy SC, Munger JW, L. Haszpra L, Barcza Z (2004) Regional carbon dioxide fluxes from mixing ratio data. Tellus 56B: 301-311.

Bakwin PS, Tans PP, Hurst DF, Zhao C (1998) Measurements of carbon dioxide on very tall towers: results of the NOAA/CMDL program. Tellus 50B: 401-415.

Bakwin PS, Tans PP, Zhao C, Ussler W, Quesnell E (1998) Measurements of carbon dioxide on a very tall tower. Tellus 47B: 535-549.

Bamberger I, Stieger J, Buchmann N, Eugster W (2014) Spatial variability of methane: Attributing atmospheric concentrations to emissions. Environ Pollut 190:65–74. doi: 10.1016/j.envpol.2014.03.028

Beck V, Chen H, Gerbig C, Bergamaschi P, Bruhwiler L, Houweling S, Röckmann T, Kolle O, Steinbach J, Koch T, Sapart CJ, van der Veen C, Frankenberg C, Andreae MO, Artaxo P, Longo KM, Wofsy SC (2012) Methane airborne measurements and comparison to global models during BARCA. J Geophys Res 117:D15310. doi: 10.1029/2011JD017345

Berhanu TA, Satar E, Schanda R, Nyfeler P, Moret H, Brunner D, Oney B, Leuenberger M (2016) Measurements of greenhouse gases at Beromünster tall tower station in Switzerland. Atmos Meas Tech 9: 2603-2614. doi:10.5194/amt-9-2603-2016

Botev ZI, Grotowski JF, Kroese DP (2010) Kernel density estimation via diffusion. Ann Stat 38: 2916–2957. doi:10.1214/10-AOS799

Brooks BGJ, Desai AR, Stephens BB, Bowling DR, Burns SP, Watt AS, Heck SL, Sweeney C (2012) Assessing filtering of mountaintop CO_2 mole fractions for application to inverse models ob biosphere-atmosphere carbon exchange, Atmos Chem Phys 12, 2099-2115. doi: 10.5194/acp-12-2099-2012

Buchwitz M, Reuter M, Schneising O, Boesch H, Guerlet S, Dils B, Aben I, Armante R, Bergamaschi P, Blumenstock T, Bovensmann H, Brunner D, Buchmann B, Burrows JP, Butz A, Chédin A, Chevallier F, Crevoisier CD, Deutscher NM, Frankenberg C, Hase F, Hasekamp OP, Heymann J, Kaminski T, Laeng A, Lichtenberg G, De Mazière M, Noël S, Notholt J, Orphal J, Popp C, Parker R, Scholze M, Sussmann R, Stiller GP, Warneke T, Zehner C, Bril A, Crisp D, Griffith DWT, Kuze A, O'Dell C, Oshchepkov S, Sherlock V, Suto H, Wennberg P, Wunch D, Yokota T, Yoshida Y (2013) The Greenhouse Gas Climate Change Initiative (GHG-CCI): Comparison and quality assessment of near-surface-sensitive satellite-derived CO_2 and CH_4 global data sets. Remote Sens Environ 162:344–362. doi: 10.1016/j.rse.2013.04.024

Cleugh H A, Raupach M R, Briggs P R, Coppin P A (2004) Regional-Scale Heat and Water Vapour Fluxes in an Agricultural Landscape: An Evaluation of CBL Budget Methods at OASIS. Boundary-Layer Meteorol 110: 99-137.

Collaud Coen M, Praz C, Haefele A, Ruffieux D, Kaufmann P, Calpini B (2014) Determination and climatology of the planetary boundary layer height above the Swiss plateau by in situ and remote sensing measurements as well as by the COSMO-2 model. Atmos Chem Phys 14: 13205-13221, doi: 10.5194/acp-14-13205-2014

Crevoisier C, Gloor M, Gloaguen E, Horowitz LW, Sarmiento JL, Sweeney C, Tans PP (2006) A direct carbon budgeting approach to infer carbon sources and sinks. Design and synthetic application to complement the NACP observation network. Tellus B 58:366–375. doi: 10.1111/j.1600-0889.2006.00214.x

Davis KJ, Bakwin PS, Yi C, Berger BW, Zhao C, Teclaw RM, Isebrands JG (2003) The annual cycles of CO_2 and H_2O exchange over a northern mixed forest as observed from a very tall tower. Glob Change Biol 9: 1278-1293.

Dlugokencky EJ, Nisbet EG, Fisher R, Lowry D (2011) Global atmospheric methane: budget, changes and dangers. Phil Trans R Soc A 369:2058–2072. doi: 10.1098/rsta.2010.0341

Eugster W, Siegrist FC (2000) The influence of nocturnal CO_2 advection on CO_2 flux measurements. Basic Appl Ecol 1:177–188. doi: 10.1078/1439-1791-00028

Frankenberg C, Bergamaschi P, Butz A, Houweling S, Meirink JF, Notholt J, Petersen AK, Schrijver H, Warneke T, Aben I (2008) Tropical methane emissions: A revised view from SCIAMACHY onboard ENVISAT. Geophys Res Lett 35: L15811. doi: 10.1029/2008GL034300

Frankenberg C, Meirink JF, van Weele M, Platt U, Wagner T (2005) Assessing methane emissions from global space-borne observations. Science 308: 1010–1014. doi: 10.1126/science.1106644

Frankenberg C, Pollock R, Lee RAM, Rosenberg R, Blavier J-F, Crisp D, O'Dell CW, Osterman GB, Roehl C, Wennberg PO, Wunch D (2015) The Orbiting Carbon Observatory (OCO-2): spectrometer performance evaluation using pre-launch direct sun measurements. Atmos Meas Tech 8: 301-313. doi:10.5194/amt-8-301-2015

Gerbig C, Körner S, Lin JC (2008) Vertical mixing in atmospheric tracer transport models: error characterization and propagation. Atmos Chem Phys 8: 591–602. doi: 10.5194/acp-8-591-2008

Gloor M, Bakwin P, Hurst D, Lock L, Draxler R, Tans P (2001) What is the concentration footprint of a tall tower? J Geophys Res 106, 17831-17840. doi: 10.1029/2001JD900021

Gohm A, Harnisch F, Vergeiner J, Obleitner F, Schnitzhofer R, Hansel A, Fix A, Neininger B, Emeis S, Schäfer K (2009) Air Pollution Transport in an Alpine Valley: Results From Airborne and Ground-Based Observations. Boundary-Layer Meteorol 131: 441-463. doi:10.1007/s10546-009-9371-9

Göckede M, Turner, DP, Michalak AM, Vickers D, Law BE (2010) Sensitivity of a subregional scale atmospheric inverse CO_2 modeling framework to boundary conditions. J Geophys Res 115: D24112. doi: 10.1029/2010D014443

Holton JR (2004) An Introduction to Dynamic Meteorology, Fourth Ed. Elsevier Academic Press, London, England, pp 535.

Imer D, Merbold L, Eugster W, Buchmann N (2013) Temporal and spatial variations of soil CO_2, CH_4 and N_2O fluxes at three differently managed grasslands. Biogeosciences 10: 5931–5945. doi: 10.5194/bg-10-5931-2013

Karion A, Sweeney C, Wolter S, Newberger T, Chen H, Andrews A, Kofler J, Neff D, Tans P (2013) Long-term greenhouse gas measurements from aircraft. Atmos Meas Tech 6: 511-526. doi:10.5194/amt-6-511-2013, 2013.

Kretschmer R, Gerbig C, Karstens U, Biavati G, Vermeulen A, Vogel F, Hammer S, Totsche KU (2014) Impact of optimized mixing heights on simulated regional atmospheric transport of CO_2. Atmos Chem Phys 14: 7149-7172. doi: 10.5194/acp-14-7149-2014.

Kuze A, Suto H, Nakajima M, Hamazaki T (2009) Thermal and near infrared sensor for carbon observation Fourier-transform spectrometer on the Greenhouse Gases Observing Satellite for greenhouse gases monitoring. Appl Opt 48: 6716-6733.

Lauvaux T, Schuh AE, Bocquet M, Wu L, Richardson S, Miles N, Davis KJ (2012) Network design for mesoscale inversions of CO_2 sources and sinks. Tellus B 64: 17980.

Lee TR, de Wekker SFJ, Sandip P, Andrews AE, Kofler J (2015) Meteorological controls on the diurnal variability of carbon monoxide mixing ratio at a mountaintop monitoring site in the Appalachian Mountains. Tellus B 67: 25659.

Lin JC, Gerbig C (2005) Accounting for the effect of transport errors on tracer inversions. Geophys Res Lett 32:L01802. doi: 10.1029/2004GL021127

Lugauer M, Winkler P (2005) Thermal circulation in South Bavaria – climatology and synoptic aspects. Meteorol Z 14: 15–30. doi: 10.1127/0941-2948/2005/0014-0015

Marquis M, Tans P (2008) Carbon Crucible. Science 320: 460–461. doi: 10.1126/science.1156451

McKain K, Wofsy SC, Nehrkorn T, Eluszkiewicz J, Ehleringer JR, Stephens BB (2012) Assessment of ground-based atmospheric observations for verification of greenhouse gas emissions from an urban region. Proc Natl Acad Sci USA. doi: 10.1073/pnas.1116645109

Merbold L, Eugster W, Stieger J, Zahniser M, Nelson D, Buchmann N (2014) Greenhouse gas budget (CO_2, CH_4 and N_2O) of intensively managed grassland following restoration. Glob Change Biol 20: 1913–1928, doi:10.1111/gcb.12518.

Miles NL, Richardson SJ, Davis KJ, Lauvaux T, Andrews AE, West TO, BandaruV, Crosson ER (2012) Large amplitude spatial and temporal gradients in atmospheric boundary layer CO_2 mole fractions detected with a tower-based network in the U.S. upper Midwest. J Geophys Res 117: G01019, doi:10.1029/2011JG001781.

Moeng C-H, Wyngaard JC (1984) Statistics of Conservative Scalars in the Convective Boundary Layer. J Atmos Sci 41(21): 3161-3169.

Moeng C-H, Wyngaard JC (1989) Evaluation of Turbulent Transport and Dissipation Closures in Second-Order Modeling. J Atmos Sci 46(14): 2311-2330.

Monin AS, Obukhov AM (1954) Basic laws of turbulence mixing in the surface layer of the atmosphere. Trudy Geof Inst AN SSSR 24: 163–187.

Myhre, G., D. Shindell, F.-M. Bréon, W. Collins, J. Fuglestvedt, J. Huang, D. Koch, J.-F. Lamarque, D. Lee, B. Mendoza, et al. (2013), Anthropogenic and Natural Radiative Forcing, in Climate Change 2013: The Physical Science Basis. Contribution of Working Group I to the Fifth Assessment Report

of the Intergovernmental Panel on Climate Change, edited by T. F. Stocker, D. Qin, et al., pp. 659–740, Cambridge University Press, Cambridge, United Kingdom and New York, NY, USA.

Nisbet E, Weiss R (2010) Atmospheric science. Top-down versus bottom-up. Science 328: 1241–1243. doi: 10.1126/science.1189936

Oney B, Henne S, Gruber N, Leuenberger M, Bamberger I, Eugster W, Brunner D (2015) The CarboCount CH sites: characterization of a dense greenhouse gas observation network. Atmos Chem Phys 15: 11147-11164. doi:10.5194/acp-15-11147-2015

Peters W, Krol MC, van der Werf GR, Houweling S, Jones CD, Hughes J, Schaefer K, Masarie KA, Jacobson AR, Miller JB, Cho CH, Ramonet M, Schmidt M, Ciattaglia L, Apadula F, Heltai D, Meinhardt F, di Sarra AG, Piacentino S, Sferlazzo D, Aalto T, Hatakka J, Strom J, Haszpra L, Meijer HAJ, van der Laan S, Neubert REM, Jordan A, Rodo X, Morgui J-A, Vermeulen AT, Popa E, Rozanski K, Zimnoch M, Manning AC, Leuenberger M, Uglietti C, Dolman AJ, Ciais P, Heimann M, Tans PP (2010) Seven years of recent European net terrestrial carbon dioxide exchange constrained by atmospheric observations. Glob Change Biol 16: 1317–1337. doi:10.1111/j.1365-2486.2009.02078.x

Pillai D, Gerbig C, Ahmadov R, Rödenbeck C, Kretschmer R, Koch T, Thompson R, Neininger B, Lavrié J V. (2011) High-resolution simulations of atmospheric CO_2 over complex terrain – representing the Ochsenkopf mountain tall tower. Atmos Chem Phys 11:7445–7464. doi: 10.5194/acp-11-7445-2011

Rotach MW, Andretta M, Calanca P, Weigel AP, Weiss A (2007) Boundary layer characteristics and turbulent exchange mechanisms in highly complex terrain. Acta Geophys 56:194–219. doi: 10.2478/s11600-007-0043-1

Rotach MW, Wohlfahrt G, Hansel A, Reif M, Wagner J, Gohm A (2013) The world is not flat - implications for the global carbon balance. Bull Am Meteorol Soc 95:1021–1028.

Schnitzhofer R, Norman M, Wisthaler A, Vergeiner J, Harnisch F, Gohm A, Obleitner F, Fix A, Neininger B, and Hansel A (2009) A multimethodological approach to study the spatial distribution of air pollution in an Alpine valley during wintertime, Atmos Chem Phys 9: 3385-3396. doi:10.5194/acp-9-3385-2009

Schuck TJ, Ishijima K, Patra PK, Baker AK, Machida T, Matsueda H, Sawa Y, Umezawa T, Brenninkmeijer CAM, Lelieveld J (2012) Distribution of methane in the tropical upper troposphere measured by CARIBIC and CONTRAIL aircraft. J Geophys Res - Atmos 117: D19304. doi: 10.1029/2012JD018199

Seibert P (1990) South foehn studies since the ALPEX experiment. Meteorol Atmos Phys 43: 91–103. doi: 10.1007/BF01028112

Smallman TL, Williams M, Moncrieff JB (2014) Can seasonal and interannual variation in landscape CO_2 fluxes be detected by atmospheric observations of CO_2 concentrations made at a tall tower? Biogeosciences 11: 735–747. doi: 10.5194/bg-11-735-2014

Stieger J, Bamberger I, Buchmann N, Eugster W (2015) Validation of farm-scale methane emissions using nocturnal boundary-layer budgets. Atmos Chem Phys 15: 14055–14069. doi:10.5194/acp-15-14055-2015

Sun J, Oncley SP, Burns SP, Stephens BB, Lenschow DH, Campos, T, Russel KM, Schimel, DS, Sacks WJ, De Wekker SFJ, Lai CT, Lamb B, Ojima D, Ellsworth PZ, Sternberg LSL, Zhong S, Clements

C, Moore DJP, Anderson DE, Watt AS, Hu J, Tschudi M, Aulenbach S, Allwine E, Coons T (2010) A multiscale and multidisciplinary investigation of ecosystem-atmosphere CO_2 exchange over the Rocky Mountains of Colorado, Bull Amer Meteorol Soc 91: 209-230

Thompson RL, Manning AC, Gloor E, Schultz U, Seifert T, Hänsel F, Jordan A, Heimann M (2009) In-situ measurements of oxygen, carbon monoxide and greenhouse gases from Ochsenkopf tall tower in Germany. Atmos Meas Tech 2: 573–591. doi: 10.5194/amt-2-573-2009

Tolk LF, Meesters AGCA, Dolman AJ, Peters W (2008) Modelling representation errors of atmospheric CO_2 mixing ratios at a regional scale. Atmos Chem Phys 8: 6587-6596, doi: 10.5194/acp-8-6587-2008

van der Molen MK, Dolman AJ (2007) Regional carbon fluxes and the effect of topography on the variability of atmospheric CO_2, J Geophys Res 112: D01104, doi:10.1029/2006JD007649

Vermeulen AT, Hensen A, Popa ME, van den Bulk WCM, Jongejan PAC (2011) Greenhouse gas observations from Cabauw Tall Tower (1992–2010). Atmos Meas Tech 4: 617–644. doi: 10.5194/amt-4-617-2011

Villani MG, Bergamaschi P, Krol M, Meirink JF, Dentener F (2010) Inverse modeling of European CH_4 emissions: sensitivity to the observational network. Atmos Chem Phys 10:1249–1267. doi: 10.5194/acp-10-1249-2010

Wanner H, Furger M (1990) The Bise - Climatology of a Regional Wind North of the Alps. Meteorol Atmos Phys 43: 105–115.

Whiteman D (2000) Diurnal mountain winds. Mountain Meteorology. Oxford University Press, New York, USA, pp 171–202.

Winderlich J, Chen H, Gerbig C, Seifert T, Kolle O, Lavrič J V, Kaiser C, Höfer A, Heimann M (2010) Continuous low-maintenance CO_2/CH_4/H_2O measurements at the Zotino Tall Tower Observatory (ZOTTO) in Central Siberia. Atmos Meas Tech 3: 1113–1128. doi: 10.5194/amt-3-1113-2010

Winderlich J, Gerbig C, Kolle O, Heimann M (2014) Inferences from CO_2 and CH_4 concentration profiles at the Zotino Tall Tower Observatory (ZOTTO) on regional summertime ecosystem fluxes. Biogeosciences 11: 2055–2068. doi: 10.5194/bg-11-2055-2014

Xiong X, Barnet CD, Zhuang Q, Machida T, Sweeney C, Patra PK (2010) Mid-upper tropospheric methane in the high Northern Hemisphere: Spaceborne observations by AIRS, aircraft measurements, and model simulations. J Geophys Res 115: D19309. doi: 10.1029/2009JD013796

Zeeman MJ, Hiller R, Gilgen AK, Michna P, Plüss P, Buchmann N, Eugster W (2010) Management and climate impacts on net CO_2 fluxes and carbon budgets of three grasslands along an elevational gradient in Switzerland. Agr For Meteorol 150: 519–530. doi: 10.1016/j.agrformet.2010.01.011

Zhang HF, Chen BZ, Machida T, Matsueda H, Sawa Y, Fukuyama Y, Langenfelds R, van der Schoot M, Xu G, Yan JW, Cheng ML, Zhou LX, Tans PP, Peters W (2014) Estimating Asian terrestrial carbon fluxes from CONTRAIL aircraft and surface CO_2 observations for the period 2006–2010. Atmos Chem Phys 14: 5807–5824. doi: 10.5194/acp-14-5807-2014

Supplementary Material: Observations of atmospheric methane and carbon dioxide mixing ratios: Tall-tower or mountain-top stations?

Ines Bamberger · Brian Oney · Dominik Brunner · Stephan Henne · Markus Leuenberger · Nina Buchmann · Werner Eugster*

* ETH Zurich, Universitätstrasse 2, 8092 Zurich, Switzerland, phone +41-44-632-6847, e-mail eugsterw@ethz.ch

S1 Management Activities at the Mountain-Top Site

Table S1 Management activities at the grasslands surrounding the FRU mountain-top station

Date in 2013	Management activity	Details
17–18 April	organic fertilizer	solid
2–8 May	grazing	suckler cows (25), calves (24)
6–14 June	grazing	cows (34)
1–2 July	cutting	0.68 ha
11–12 July	cutting	0.71 ha
18 July	organic fertilizer	solid
23 July	cutting	3.28 ha
24 July	organic fertilizer	liquid
2–4 September	cutting	0.68 ha
23 September–2 October	grazing	cows (34)
7–13 November	grazing	sheep (15)

S2 Origin of Methane Emissions

To determine whether the local methane sources at the mountain-top station are diffuse or attributable to a specific source we analyzed the dependence of the between-site differences ($\Delta C_m = C_{m,\mathrm{FRU}} - C_{m,\mathrm{BER}}$) on the wind direction at the mountain top (FRU). This was done both for two-hourly average CH_4 mixing ratios and for the 5th percentiles of the two-hourly frequency distribution (Fig. S1). For average CH_4 mixing ratios these differences remained generally below 0.02 ppm for any wind direction, except for southerly winds from the direction of the ETH research station when average mixing ratios at the FRU were considerably higher (up to 0.065 ppm).

This pattern was not restricted to dates when cattle were grazing on the pastures surrounding the FRU measurement station, thus indicating the general influence of CH_4 emissions from the nearby farmstead in the south. Evaluating the between-site differences for the 5th percentiles instead of the average mixing ratios, however, showed no comparable dependence on wind direction (Fig. S1). Thus the percentile approach, which assumes that the lower edge of the two-hourly frequency distribution is mainly unaffected by local greenhouse gas fluxes, was successful in eliminating the most prominent influences on CH_4 mixing ratios imposed by the local farmstead.

S3 Analyzing Mixing Ratio Differences

In order to find the most likely predictor variables that influence the mixing ratio difference between the FRU (mountain-top) and BER (tall-tower) sites, we carried out a principal component analysis

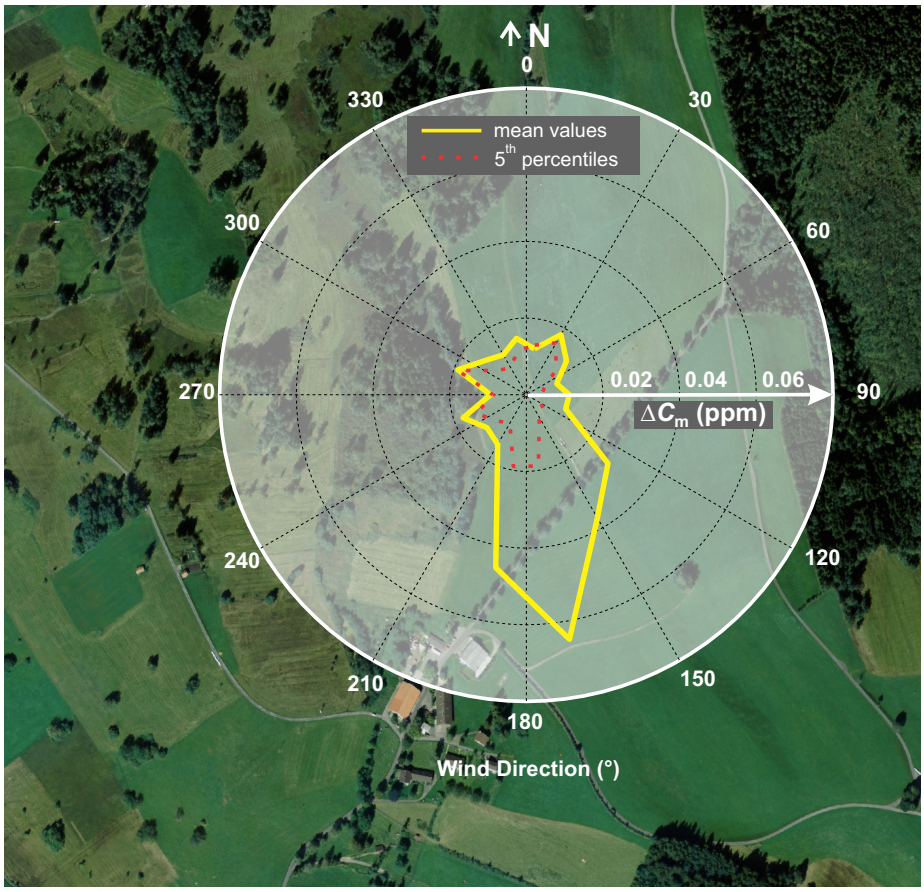

Fig. S1 Binned averages of the CH_4 differences between the FRU mountain-top station and the BER tall-tower station (ΔC_m) as calculated from the annual time series of 2-h averages (yellow line) and the 5th percentiles of the 2-h frequency distribution (red dotted line) for 20° bins of the wind direction at the mountain top, overlaid on an orthoimage © 2014 swisstopo (JD100042) of the mountain-top site

(not shown) to detect collinearities among the meteorological variables that have the potential to predict such differences, and then performed an analysis of variance to determine, which groups of environmental conditions can be used to classify mixing ratio differences between FRU and BER. All statistical analyses were done with R (R Core Team, 2016).

The response variables of interest were ΔC_m and ΔC_c, the absolute differences in CH_4 and CO_2 mixing ratio measurements, respectively, measured at the two sites. Positive values of ΔC_m and ΔC_c indicate that the respective gas mixing ratio measured at the FRU mountain-top site exceeded the concurrent measurements at the top of the BER tall-tower site.

S3.1 Analysis of Variance

S3.1.1 Material and Method

We carried out an analysis of variance to quantify the differences between the FRU and BER mixing ratio measurements. The goal was not primarily to determine the offset between the sites, but how this potential offset varies with the variables used in the principal component analysis. We used a three-step procedure that takes into account that different variables are most relevant for ΔC_m than for ΔC_c:

1. A five-factorial analysis of variance was computed with the variables wind direction (ϑ), horizontal wind speed (U), atmospheric stability (z/L; all measured at FRU), H_r (hour of day),

and S_n (season, starting with 12 levels corresonding to calender months). To simplify calculations, all variables were binned to classes to reduce the number of levels. In the first step no interactions between the different variables were considered. The H_r variable was binned at 2-h resolution, and atmospheric stability was aggregated to the three classes "unstable" ($z/L <$ –0.0625), "neutral" (–0.0625 $\leq z/L <$ 0.0625), and "stable" ($z/L \geq$ 0.0625), since both z/L and L/z only showed a weak effect in both principal component analyses for ΔC_m and ΔC_c. Wind speed was binned into classes at intervals of 1 m s^{-1}, and ϑ (as measured at the FRU site) was binned in 10° segments. Tukey's honest significant difference test was calculated on all groupwise comparisons of mixing ratio differences.

2. After this, the classes without significant in-between differences were combined to reduce the number of classes in each variable. U was aggregated to five classes (0–1 m s^{-1}, 1–2 m s^{-1}, 2–5 m s^{-1}, 5–6 m s^{-1}, $>$6 m s^{-1} for ΔC_m, and $<$ 1 m s^{-1}, 1–2 m s^{-1}, 2–4 m s^{-1}, 4–6 m s^{-1}, $>$ 6 m s^{-1} for ΔC_c). ϑ was aggregated to three classes (70–120°, 120–200°, 200–70°). To use a more detailed resolution of H_r and S_n than in Fig. 8, an aggregation was done as shown in Fig. S2 with four classes each for H_r and S_n.
3. With this reduced set of classes a full analysis of variance model including interactions was run. Using stepwise exclusion, all nonsignificant variables and interactions (adjusted $p \geq 0.05$) were subsequently eliminated from the model. Within a few iterations we were left with a simplified analysis of variance model that only contained variables and interactions that showed a nonzero influence on measured ΔC_m or ΔC_c, respectively, at adjusted $p < 0.05$ (see Tables S2 & S3).

S3.1.2 Results

On average the mixing ratio offset between FRU and BER was 0.019 ± 0.019 ppm for ΔC_m, and 2.9 ± 3.7 ppm for ΔC_c (mean difference $\pm$ standard deviation of all group comparison of the groups that were used in the final analysis of variance model).

Differences in CH_4 mixing ratios.

In the first step (no interactions considered) an aggregation of predictor classes was possible, namely H_r could be reduced to two classes: 0800–1600 UTC (day), and 2000–0400 UTC (night). Transition times were not included in the analysis. The 12 months of S_n could be aggregated to four seasons, January, February–July, August, and September–December. January and August differed in all comparisons with other months, hence this site-specific classification was chosen (Fig. S2). Wind speed classes could be reduced to five classes, and ϑ was aggregated to three classes (see above). The two stability groups "unstable" and "neutral" did not differ significantly and thus were combined. These classes were used in step 3 to obtain the final analysis of variance Table S2.

The output from the final analysis of variance model (Table S2) was then used to compute group averages, standard deviations, and standard error of the mean of ΔC_m to quantify the possible local effects on ΔC_m. These averages were then ranked and plotted in Fig. S3 in combination with the predictor classes involved.

Figure S3 shows quite clearly that wind directions from 120–200° were mostly responsible for the largest positive deviations, i.e., local emissions at FRU increase CH_4 mixing ratios above the value expected at BER. Contrastingly, the most negative deviations are associated with the highest wind speeds and with the early season (February to July).

Wind directions from 70–120° (Bise winds; Wanner and Furger, 1990) never led to significantly increased ΔC_m compared to other factor combinations, and hence those wind directions can be considered representative for BER conditions, irrespective of H_r, S_n, U, and z/L. Whereas stability, U, and H_r had a similar influence on the variability of ΔC_m (F ratios in the range 40–50, Table S2), only U showed a distinct influence on average ΔC_m. While weak winds led to positive ΔC_m, strong winds were usually associated with negative ΔC_m. Thus, U – which is also related to stability – had a much stronger influence than stability on local anomalies in CH_4 mixing ratio measurements at FRU.

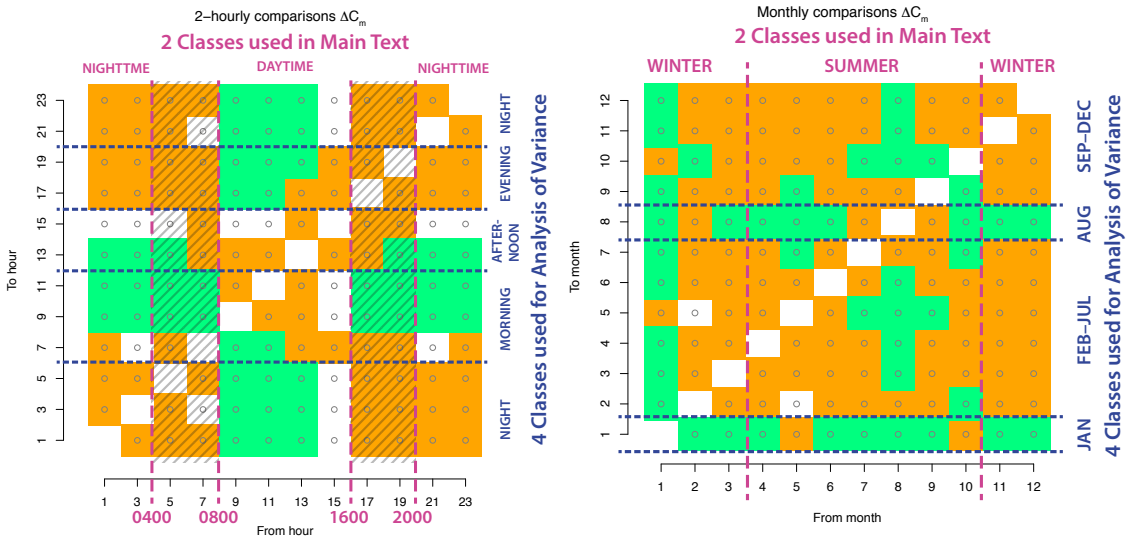

Fig. S2 Aggregation of hour of day (H_r, left) and season (S_n, right) for the analysis of variance of CH_4 mixing ratio differences. Both panels show a graphical matrix of pairwise comparisons of CH_4 mixing ratio differences. Orange cells denote that Tukey's honest significant difference test yielded an adjusted $p > 0.05$, whereas green cells show highly significant differences (adjusted $p < 0.01$). White cells are either significant in the range $0.01 \leq$ adjusted $p \leq 0.05$, or are the diagonal of the matrix which is ignored. The vertical dashed lines show the coarse separation of the classes used in Fig. 8, whereas the horizontal dashed lines show the separations between classes used in this additional analysis of variance (Fig. S3 and Table S2). The hashed areas are the transition times that are excluded in the analysis for Fig. 8, but are included in the analysis of variance Table S2

Mean ΔC_m was 0.019 ± 0.019 ppm, shown in Fig. S3 with the two dashed vertical lines. The most positive ΔC_m ranged up to 0.060 ppm (January, neutral z/L, calm winds $< 1\,\mathrm{m\,s^{-1}}$, and ϑ 120–200°), and the most negative ΔC_m was –0.045 ppm (afternoons with relatively strong winds with U in the range 7–8 $\mathrm{m\,s^{-1}}$).

Differences in CO_2 mixing ratios.

For ΔC_c the aggregation of the variables led to slightly different classes than for ΔC_m. For simplicity we used the same H_r classes as for CH_4 (night 2000–0600 UTC, morning 0600–1200 UTC,

Table S2 Analysis of variance table for the response variable ΔC_m after stepwise elimination of nonsignificant predictors and predictor combinations, sorted by F value

Factor Interaction	Df	Sum Sq	Mean Sq	F value	Pr($>F$)	
ϑ	2	0.6538	0.32691	249.6591	$< 2.2{\cdot}10^{-16}$	***
z/L	1	0.0648	0.06476	49.4552	$2.398{\cdot}10^{-12}$	***
U	7	0.3946	0.05638	43.0564	$< 2.2{\cdot}10^{-16}$	***
H_r	3	0.1575	0.05249	40.0872	$< 2.2{\cdot}10^{-16}$	***
S_n	3	0.1117	0.03724	28.4392	$< 2.2{\cdot}10^{-16}$	***
$\vartheta : U$	6	0.0728	0.01213	9.2623	$4.227{\cdot}10^{10}$	***
$\vartheta : z/L$	2	0.0211	0.01054	8.0496	0.0003247	***
$S_n : H_r$	9	0.0477	0.00530	4.0448	$3.561{\cdot}10^{-5}$	***
$\vartheta : H_r$	6	0.0249	0.00415	3.1680	0.0042138	**
$\vartheta : S_n : U$	23	0.0703	0.00306	2.3333	0.0003198	***
$\vartheta : H_r : z/L$	9	0.0238	0.00265	2.0236	0.0330805	*
$\vartheta : S_n : H_r$	23	0.0504	0.00219	1.6732	0.0230944	*
Residuals	3783	4.9535	0.00131			

Asterisks in the last column indicate $p < 0.001$ (***), $p < 0.01$ (**), and $p < 0.05$ (*), and the colons in the first column indicate interactions among variables. The following classes were built for each variable: wind direction ϑ 70–120°, 120–200°, 200–70°; wind speed $U < 1\,\mathrm{m\,s^{-1}}$, 1–2 $\mathrm{m\,s^{-1}}$, 2–5 $\mathrm{m\,s^{-1}}$, 5–6 $\mathrm{m\,s^{-1}}$, $> 6\,\mathrm{m\,s^{-1}}$; hour of day H_r 0600–1200 (morning), 1200–1600 (afternoon), 1600–2000 (evening), 2000–0600 (night); season S_n January, February–July, August, September–December; stability z/L stable, unstable and neutral.

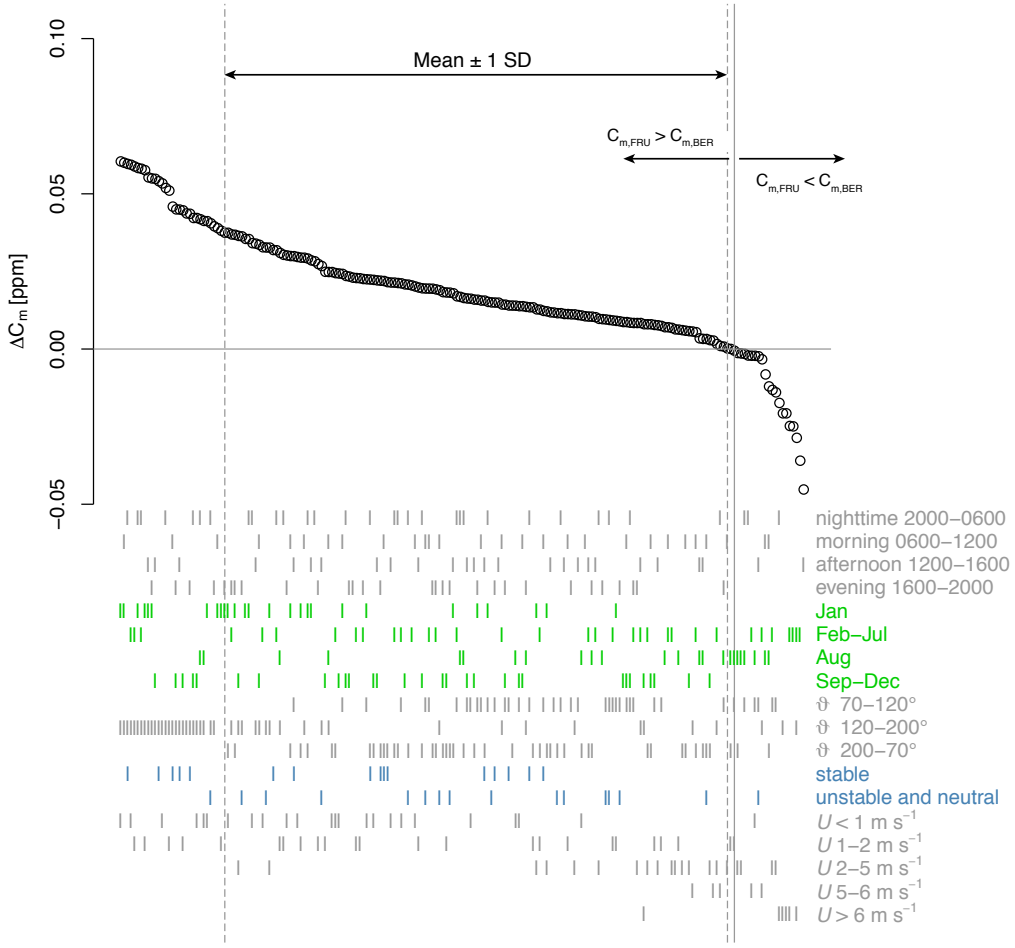

Fig. S3 Group averages of differences in CH_4 mixing ratios measured at the FRU site in comparison with the BER site, sorted in descending order. The mean difference $\pm$ one standard deviation (i.e., 0.019 ± 0.019 ppm) is shown with two vertical dashed lines. The zero difference is shown with a horizontal and a vertical solid thin line. The vertical symbols below the graph indicate which class combination was used for the respective group average. As a reading example: the most positive values of ΔC_m are found in group comparisons that involve the wind direction sector 120–200°, and the most negative deviations are found at the highest wind speeds

afternoon 1200–1600 UTC, evening 1600–2000 UTC), and the transition times (0400–0800 UTC and 1600–2000 UTC) were excluded from further analysis (Fig. S4) in the same way as was done with CH_4. Seasonality was represented by four levels: November–April, May–June, July–August, and September–October. For ϑ we used the same three sectors as for CH_4: ϑ 70–120°, 120–200°, 200–70°. For U five levels were used: < 1 m s^{-1}, 1–2 m s^{-1}, 2–5 m s^{-1}, 5–6 m s^{-1}, and > 6 m s^{-1}. Stability had three levels: "unstable", "neutral", and "stable". The final analysis of variance model is shown in Table S3.

Similarly to ΔC_m we sorted the differences and plotted the values along with the classes involved (Fig. S5). Beginning at the bottom of Fig. S5 it is quite clearly seen that large positive differences are never associated with wind speeds above 2 m s^{-1}, and the most negative deviations are associated with high wind speeds (and thus enhanced turbulent mixing). At the same time, the most negative values of ΔC_c tend to be related to the southeastern wind sector. This wind sector is mostly associated with foehn conditions (Desai et al., 2016), that bring fresh and warm air from the Alps directly to FRU, whereas the BER site actually should already see parts of the anthropogenic emissions in the Alpine foreland. Hence such differences—although weak and only represented by few datapoints—are realistic and most likely true differences, not sampling artefacts. Very positive deviations are primarily associated with nighttime or early morning (dusk), and mostly during

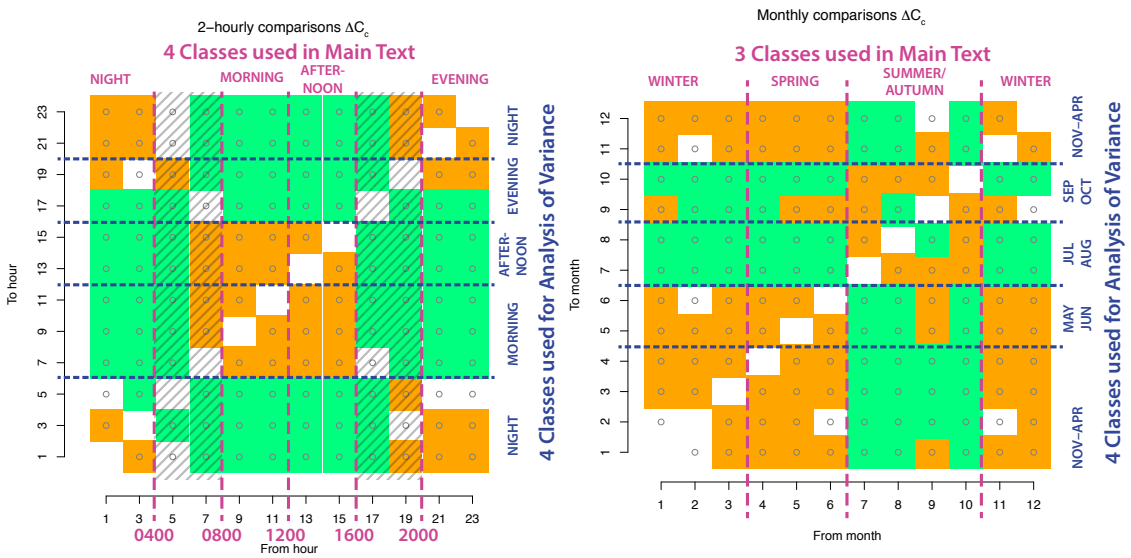

Fig. S4 Aggregation of hour of day (H_r, left) and season (S_n, right) for the analysis of variance of CO_2 mixing ratio differences. Both panels show a graphical matrix of pairwise comparisons of CO_2 mixing ratio differences. Orange cells denote that Tukey's honest significant difference test yielded an adjusted $p > 0.05$, whereas green cells show highly significant differences ($p < 0.01$). The vertical dashed lines show the coarse separation of the classes used in Fig. 9, whereas the horizontal dashed lines show the separations between classes used in this additional analysis of variance (Fig. S5 and Table S3). The hashed areas are the transition times that are excluded in the analysis for Fig. 9, but are included in the analysis of variance Table S3. White cells are either the diagonal of the matrix or differences in the range $0.01 < p \leq 0.05$

Table S3 Analysis of variance table for the response variable ΔC_c after stepwise elimination of nonsignificant predictors and predictor combinations, sorted by F value

Factor Interaction	Df	Sum Sq	Mean Sq	F value	Pr($>F$)	
H_r	3	20553	6851.2	363.5365	$<2.2{\cdot}10^{-16}$	***
ϑ	2	8716	4357.8	231.2329	$<2.2{\cdot}10^{-16}$	***
U	4	7569	1892.3	100.4102	$<2.2{\cdot}10^{-16}$	***
S_n	3	5265	1755.2	93.1325	$<2.2{\cdot}10^{-16}$	***
z/L	2	2767	1383.3	73.4019	$<2.2{\cdot}10^{-16}$	***
$S_n : H_r$	9	7604	844.9	44.8299	$<2.2{\cdot}10^{-16}$	***
$\vartheta : S_n$	6	4141	690.1	36.6186	$<2.2{\cdot}10^{-16}$	***
$H_r : z/L$	6	699	116.5	6.1814	$1.823{\cdot}10^{-6}$	***
$H_r : U$	12	893	74.4	3.9496	$4.379{\cdot}10^{-6}$	***
$S_n : U$	11	778	70.8	3.7547	$2.296{\cdot}10^{-5}$	***
$\vartheta : H_r$	6	376	62.6	3.3243	0.002882	**
$\vartheta : S_n : H_r$	16	710	44.4	2.3547	0.001751	**
$\vartheta : S_n : U$	19	768	40.4	2.1435	0.002731	**
$S_n : H_r : z/L$	16	615	38.4	2.0390	0.008491	**
$\vartheta : H_r : z/L$	12	436	36.3	1.9285	0.026884	*
$\vartheta : S_n : z/L$	22	794	36.1	1.9150	0.006244	**
$\vartheta : S_n : z/L : U$	51	1564	30.7	1.6275	0.003339	**
Residuals	3689	69522	18.8			

Asterisks in the last column indicate $p < 0.001$ (***), $p < 0.01$ (**), and $p < 0.05$ (*), and the colons in the first column indicate interactions among variables. The following classes were built for each variable: wind direction ϑ 70–120°, 120–200°, and 200–70°; wind speed $U < 1\,\mathrm{m\,s^{-1}}$, 1–2 $\mathrm{m\,s^{-1}}$, 2–4 $\mathrm{m\,s^{-1}}$, 4–6 $\mathrm{m\,s^{-1}}$, $> 6\,\mathrm{m\,s^{-1}}$; hour of day H_r 0600–1200 (morning), 1200–1600 (afternoon), 1600–2000 (evening), 2000–0600 (night); season S_n November–March, April–June, July–August, September–October; stability z/L stable, neutral, unstable.

the warm season from July until October. This coincides with the period when the vegetation is most active during the day. At the same time soils are warm enough to enhance the activity of soil microbes that decompose soil organic matter and increase the local CO_2 mixing ratio, namely at night. The largest positive ΔC_c observed was 14.3 ppm (July–August, neutral z/L, calm winds

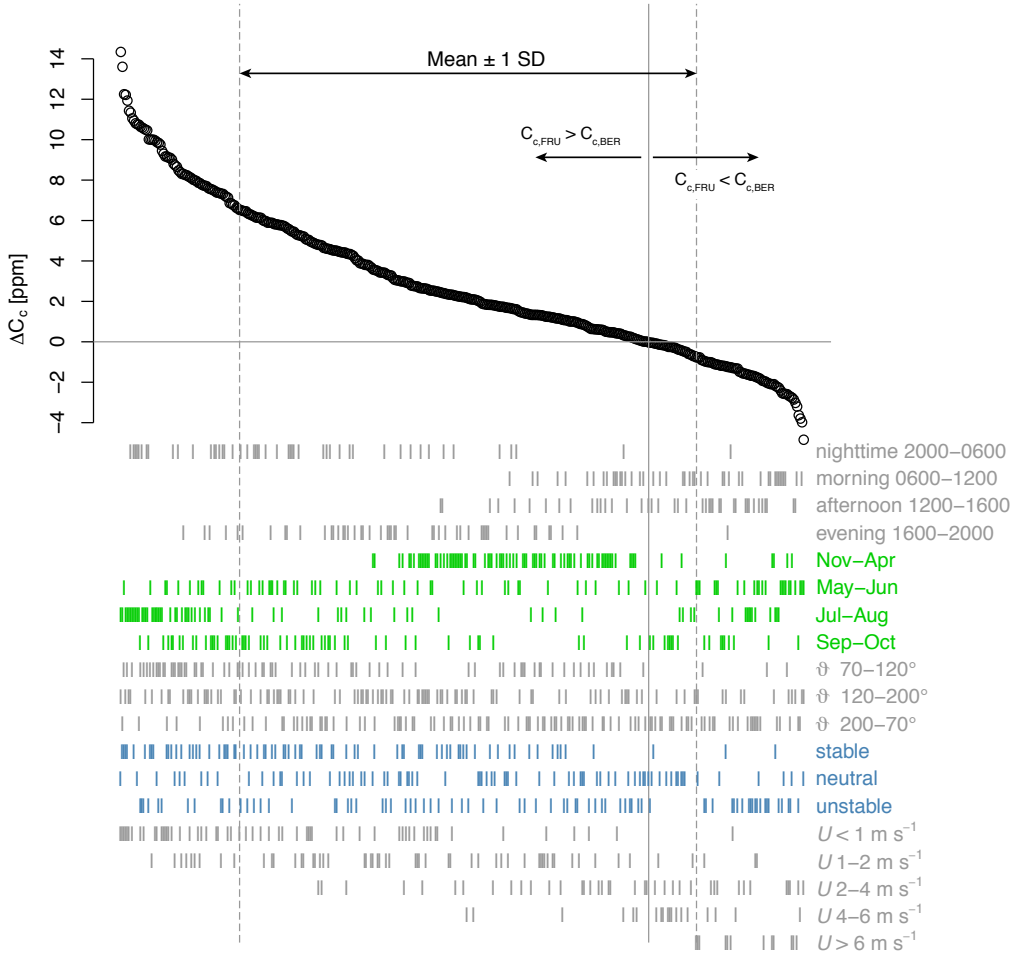

Fig. S5 Group means of differences in CO_2 mixing ratios measured at the FRU site in comparison with the BER site, sorted in descending order. Only group comparisons with statistically significant nonzero differences ($p < 0.05$) are shown. The mean difference $\pm$ one standard deviation (i.e., 2.9 ± 3.7 ppm) is shown with two vertical dashed lines. The zero difference is shown with a horizontal and a vertical solid thin line. The vertical symbols below the graph indicate which class combination was used for the respective group mean

$< 1\,\mathrm{m\,s^{-1}}$, and ϑ 120–200°), and the most negative value was –4.8 ppm (May–June, neutral z/L, U 2–4 $\mathrm{m\,s^{-1}}$, and ϑ 120–200°).

References

Desai AR, Wohlfahrt G, Zeeman MJ, Katata G, Eugster W, Montagnani L, Gianelle D, Mauder M, Schmid HP (2016) Montane ecosystem productivity responds more to global circulation patterns than climatic trends. Environ Res Lett 11:024,013, DOI 10.1088/1748-9326/11/2/024013

R Core Team (2016) R: A Language and Environment for Statistical Computing. R Foundation for Statistical Computing, Vienna, Austria, URL https://www.R-project.org/

Wanner H, Furger M (1990) The Bise – Climatology of a regional wind north of the Alps. Meteorol Atmos Phys 43:105–115, DOI 10.1007/BF01028113